International Journal of Greenhouse Gas Control 126 (2023) 103906

Contents lists available at ScienceDirect

International Journal of Greenhouse Gas Control

journal homepage: www.elsevier.com/locate/ijggc

Gas leakage from abandoned wells: A case study for the Groningen field in the Netherlands

Al Moghadam *, Elisabeth Peters, Susanne Nelskamp

TNO, Applied Geosciences, the Netherlands

ARTICLE INFO

Keywords:
Well leakage
Aquifers
Abandoned wells
Cement damage
Methane plume
Groningen

ABSTRACT

The Groningen gas field in the Netherlands has been a major source of natural gas in Europe for the past few decades. There are approximately 350 wells drilled in the field that either already are or will be plugged and abandoned in the near future. In this work, we developed a two-phase, two-component numerical model based on the stratigraphy and the petrophysical data from a well in the Groningen field. The focus was to estimate the magnitude of methane leakage from the abandoned reservoir and the shallow gas-bearing formations. Methane is a potent greenhouse gas and fugitive methane emission from abandoned wells is of concern. The results indicate that highly depleted reservoirs are not a likely source of leakage, as long as they are not re-pressurized. However, shallow gas-bearing formations capable of bulk gas flow can pose a significant leakage risk. Permeable intermediate formations between the gas source and freshwater aquifers can act as a buffer zone, reducing the maximum rate of leakage into the atmosphere/aquifer system. For a mildly damaged cement sheath (1 mD) with a viable gas source, the leakage rate is relatively small (less than 30 kg/year of methane). The high leakage rate scenario results in a leakage rate as high as 4500 kg/year, with a methane plume in the freshwater aquifer that extends up to 450 m away from the well after 100 years. The results of this study can be used to identify wells that are at a higher risk of gas leakage, and the relative consequence of such phenomena on greenhouse gas emissions and local freshwater quality.

1. Introduction

The oil and gas industry is responsible for significant levels of methane emission in the atmosphere through deliberate flaring and venting or unintentional fugitive leakages through equipment and wellbores (Bachu, 2017). Fugitive emissions have been reported as a significant source of GHG emissions in Canada (Conference Board of Canada, 2011), United States (US EPA, 2017; Kang et al., 2016; Omara et al., 2016), and the North Sea (Vielstadte et al., 2015, 2017; Bottner et al., 2020). Fugitive emissions include leakage along or through active or abandoned wells. Aside from being a source of GHG emissions, methane leakage along wells could contaminate shallow water sources (Harrison, 1983; Kelly et al., 1985; Sherwood et al., 2016; Darrah et al., 2014; Osborn et al., 2011). The cause and magnitude of well leakage need to be understood, to enable governments to set effective policies in mitigating fugitive emissions.

There are several types of cement failure that could occur in a wellbore, jeopardizing the cement integrity. The cement can debond from the casing or the formation, creating what is called a "microannulus" (Gasda et al., 2004; Roy et al., 2018; Moghadam et al., 2022). Cement can also undergo shear failure, tensile cracks, and disking (horizontal cracks in the cement sheath which are not generally considered to be a leakage risk) depending on the downhole conditions and cement properties (Bois et al., 2011; King and King, 2013). Cement failure, particularly a microannulus, can provide a leakage pathway for methane to flow upwards along the well. However, the mere presence of a flow pathway is not sufficient to cause a leak. A source of gas and sufficient pressure gradient are also necessary conditions for well leakage to occur.

Direct measurement of methane leakage along wellbores is a challenging task. A leak might not be detectable at the surface but could still contaminate shallow groundwater (Schout et al., 2020). Numerical modeling can assist in understanding the mechanisms of gas leakage along abandoned wells and the important parameters that control the leakage rate. In addition, numerical modeling can be used to design more effective monitoring strategies. Several studies exist in the literature that use modeling to understand the consequences of well leakage (Nowamooz et al., 2015; Caroll et al., 2014; Postma et al., 2019). Some

* Corresponding author.
E-mail address: al.moghadam@tno.nl (A. Moghadam).

https://doi.org/10.1016/j.ijggc.2023.103906
Received 19 September 2022; Received in revised form 1 May 2023; Accepted 6 May 2023
Available online 17 May 2023

studies investigate the rate of leakage and its sensitivity to important geological and wellbore parameters (Rice et al., 2018; Nowamooz et al., 2015; Reagan et al., 2015), others have attempted to use modeling coupled with field measures of leakage to estimate the permeability of leakage pathways (Tao and Bryant, 2014; Kang et al., 2015). The former provide important lessons in modeling techniques and analyses, and the latter provide clarity on the input parameters for the numerical models. Most leakage studies, however, focus on CO_2 leakage along wellbores in the context of carbon sequestration (Harvey et al., 2013; Keating et al., 2014).

1.1. Numerical studies

Carroll et al. (2014) describes the impact of CO_2 leaks along abandoned wells on shallow aquifers. They assumed various levels of CO_2 leakage and simulated the impact on an aquifer using a 2D, multiphase reactive simulator. They did not model the CO_2 flow along the wellbore itself, or the impact of other permeable formations between the target and the aquifer. They concluded that CO_2 leakage could significantly change the pH of groundwater; however, the plume will not reach far distances and the risk should be limited. Postma et al. (2019) estimated the field scale leakage of CO_2 through abandoned legacy wells. They created a hypothetical scenario of a CO_2 injector surrounded by a large number of leaky abandoned wells. They reported that CO_2 leakage as a percentage of the total CO_2 injected will be small over a long timeframe.

Nowamooz et al. (2015) conducted numerical simulations to investigate the impact of methane leakage along an abandoned shale gas well in Quebec, Canada. The model included both advective and diffusive flow mechanisms. Conceptually the model included a cement section that connected all the formations to the base of an aquifer. The aquifer itself was not included in the model and the impact of shallow gas pockets was not considered. Their results show that if cement quality is adequate (permeability less than 1 mD) the leak rates will be less than 0.01 m^3/day which is below the minimum reported vent flow in Quebec. In that case, the permeability of the target formation does not impact the leakage rate. However, when cement quality is poor (permeability above 10 mD) the target formation's permeability can become important and lead to higher leakage rates. Their model did not provide the details of methane dissolved in the aquifer and the evolution of the plume. Schout et al. (2020) studied the impact of groundwater flow on the retention of methane leakage in a shallow aquifer. They assumed a fixed leak rate through a small area at the base of an aquifer. They concluded that depending on the groundwater velocity, leakage rate, and flow properties of the formation, methane can be retained in the aquifer for years or decades before reaching the surface. In their work, flow along the abandoned well and the impact of shallow gas pockets and brine formations were not included. Reagan et al. (2015) conducted a comprehensive sensitivity analysis to investigate the impact of fractures/faults and well integrity failure on methane leakage from tight gas wells. The model geometry assumed that the well connects the target formation to the shallow aquifer. The overburden was assumed to be impermeable. They concluded that the cement permeability and the target formation pressure and permeability were the most consequential parameters in determining gas leakage into the aquifer. They noted that in all their cases water flowed downwards along the leaky well. Roy et al. (2016) used a reactive transport simulator to investigate the attenuation of dissolved methane in water for confined and unconfined aquifers. They concluded that in both confined and unconfined aquifers methane oxidation could attenuate a migrating dissolved methane plume. This effect was stronger in unconfined aquifers. However, this natural attenuation is sensitive to the leak rate and duration, and the background geochemistry present in the water. Rice et al. (2018) investigated methane leakage into an aquifer from a source 20–30 m below the aquifer's base. Their base case shows plume diameter of 350 m at the base of the aquifer after 100 years. They ran a sensitivity analysis and emphasized the need for two-phase flow modeling and accurate estimates of relative permeabilities and capillary pressure relationships.

Numerical studies in the literature point to the fact that the average cement sheath permeability is one of the most critical parameters controlling the leak rate. Matrix permeability of intact cement is reported to be less than 1 μD (Stormont et al., 2018; Bachu and Bennion, 2009; Meng et al., 2021). Therefore, it should provide an effective barrier to flow if the cement is perfectly bonded to the casing and the formation. However, documented presence of leaky wells indicates loss of seal capacity in some cases. Crow et al. (2010) and Gasda et al. (2013) analyzed the cement integrity of several wells using a Vertical Interference Test (VIT). This test measures the hydraulic connection between the annular cement across a section of the well. Gasda et al. (2013) reported a range of 1 to 100 mD for the effective permeability of the cement sheath behind the casing from 3 datasets, while Crow et al. (2010) estimated a value between 0.5 to 1 mD for a single well. Tao and Bryant (2014) used surface casing pressure (SCP) and surface casing vent flow (SCVF) data from 300 oil and gas wells in combination with a Monte-Carlo simulation technique to estimate the effective permeability of the annular cement. Their results indicate that annular cement permeability could vary between 0.01 and 10 mD. Kang et al. (2015) used methane emission data from 42 wells in Pennsylvania to estimate the effective annular permeability of the abandoned wells. Their results indicate a range of 10^{-6} to 10^{2} mD for the leakage pathway permeabilities. Their database included both plugged and unplugged wells. For unplugged wells, the effective permeability estimates refer to the combination of flow paths inside and outside the wells. The effective permeability for the plugged wells ranged between 10^{-4} and 10^{1} mD, with an average of 0.4 mD. Moghadam et al. (2022) reported a range of 0.5 to 100 mD (equivalent to a microannulus aperture of 10 to 50 microns) for the cement sheath permeability. Their study analyzed leakage measurements from 10 datasets in the literature, each including 19 to 147 wells. The measurements were conducted at the wellhead using a static chamber methodology.

1.2. Field evidence

Several studies have collected field evidence of well leakage in different jurisdictions (Bachu, 2017; Davies et al., 2014; Ingraffea et al., 2014; Kang et al., 2014). Two approaches have been used to investigate potential leakage in active and abandoned wells. The first approach is field campaigns, where potential leakage fluxes are measured by sampling at the surface, in the unsaturated zone or the groundwater (Schout et al., 2019; McMahon et al., 2018; Kang et al., 2016; Williams et a., 2020). The second approach is desk campaigns, where a large amount of data is analyzed to find evidence of well failure (Davies et al., 2014; Bachu 2017; Watson and Bachu, 2009). The data is typically collected by the local authority overseeing the operation and maintenance of oil and gas wells. Several studies spanning more than a decade have analyzed the leakage data reported to the Alberta Energy Regulator (AER) in Canada (Bachu and Watson, 2006; Watson and Bachu, 2008, 2009; Bachu, 2017; Abboud et al., 2021). As of 2013, nearly 7% of the 450,000 wells in Alberta (including conventional and thermal oil and gas wells) show some form of gas leakage. The reported data is a qualitative indication of leakage in the form of sustained casing pressure (SCP), sustained casing vent flow (SCVF), and gas migration (GM) outside the casing. Watson and Bachu (2009) determined that the leakage pathways are predominately due to time-independent mechanical factors during completion, operations, and abandonment. These factors can lead to cement failure which allows for gas to flow upwards. 559 wells in the AER database included gas source analyses (Bachu, 2017). Most of the wells (98.5%) show gas leakage from a formation at a shallower depth than the target formation. Their results show that in most cases, mechanical failure of cement outside the casing provides the leakage pathway for methane, while the source of leakage is likely the shallower gas formations (such as coal beds) that are hydrostatic or over-pressured (Bachu, 2017).

Schout et al. (2019) analyzed surface methane concentrations at 29 abandoned well sites in the Netherlands (1 oil and 28 gas wells). They identified 1 well out of 29 that leaks methane due to well integrity failure (3.4%). They estimated a methane leakage rate of 3880 kg/year at 2 m depth below the surface. The methane was of thermogenic origin likely from the Holland Greensand Member, a gas bearing formation in the Netherlands at a depth of 1420 to 1481 m. The target formation (Monster Formation) is at a depth of 2800 to 3000 m. Their investigation shows that for the cut and buried wells, surface measurements of methane concentration may not identify existing leakages. Gas dispersion in the unsaturated zone with (aerobic) methane oxidation reduces the methane concentration significantly. Williams et al. (2021) statistically analyzed 598 direct methane emission measurements from abandoned oil and gas wells across US and Canada. They reported leakage rates ranging between 0.016 and 420 kg/year with an average of 53 kg/yr. Pekney et al. (2018) measured methane leakage at 31 well sites in Pennsylvania. 22 wells showed some level of leakage at the wellhead at an average of 250 kg/year. The measurements were repeated after 2 years on high-emitting wells and the results indicate that flow rates are sustained through time. El Hachem and Kang (2022) conducted 85 measurements of CH4 and H2S emission rates from 63 gas wells in Ontario, Canada. Their results indicate that methane emissions from abandoned plugged wells in the region are underestimated by a factor of 920.

Osborn et al. (2011) analyzed samples from shallow groundwater systems overlying the Marcellus shale in Pennsylvania and Utica shale in New York. They reported an average methane concentration of 19.2 mg/L in water wells within 1 km of a gas well, likely thermogenic in origin. An average of 1.1 mg/L was observed in wells that were in nonactive areas, with predominantly biogenic origin. McMahon et al. (2018) analyzed water samples from 15 monitoring wells in Colorado over a period of 7 years (2011–2016). Three of these wells were within 50 m of an abandoned gas well. Thermogenic methane at high concentrations between 16 and 20 mg/L was found in one of the wells. Methane concentration did not materially change over the seven-year duration of the study.

1.3. Present study

The field evidence indicates that in most regions only a small fraction of wells leaks significantly. The leak could be into the freshwater aquifers, the atmosphere, or both. Additionally, the field scale measurements indicate that in most cases the source of leakage is a gas bearing formation above the target formation (Schout et al., 2019; Bachu, 2017). This is an important realization that is largely missing from the current modeling studies. In addition, the presence of permeable brine formations above the source formation might add another layer of complexity. These formations could allow methane storage, dampening the impact of leakage on the shallow freshwater aquifers. There are at least three interconnected systems at play during methane leakage along a wellbore. The source formation could be the abandoned formation or a shallower formation, or both. Methane flows out of the source formation into the leakage pathway, e.g., the annular cement. If other permeable formations are present, there could be methane or brine exchange between them and the leaky wellbore. The leaking methane could reach shallow aquifers and develop a moving plume through advective and diffusive flow processes over a long timeframe. Fig. 1 illustrates a schematic of the interconnected subsurface systems that could contribute to methane contamination.

In this study, we aim to investigate the potential for methane leakage from an abandoned well in the Groningen Field, in the Netherlands. We estimate the magnitude of gas leakage and the extent of the dissolved methane plume in local shallow aquifers over time. The impact of various levels of cement damage, diffusion, buoyancy, and formation properties are investigated. Presence of shallow gas-bearing formations is also considered, which is missing from the literature. This study is conducted using a numerical model and includes freshwater aquifers, the underlying formations down to the gas target, and the leakage pathway (wellbore cement). The results enable regulators and operators to understand the potential extent of methane contamination of aquifers over time and judge the necessity of a mitigation strategy. In addition, understanding the expected radius and concentration of the methane plume can assist with the design of monitoring campaigns. Particularly, the rate and location of water sampling needed to monitor the methane levels in aquifers.

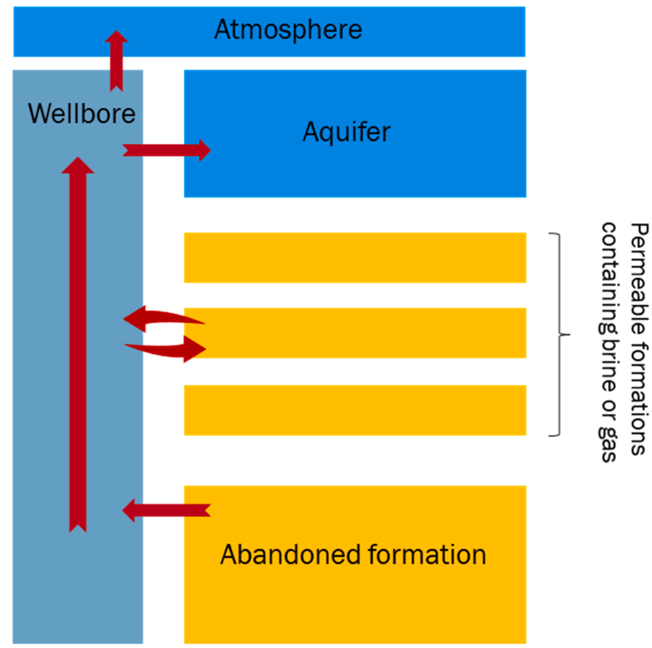

Fig. 1. A schematic of the subsurface flow pathways contributing to leakage to the shallow aquifers.

2. Groningen geological setting

The Groningen Gas Field was selected as the case study area for the present work. More than 350 wells have been drilled during the lifetime of the field that are now in various stages of their life and abandonment. Several other hydrocarbon fields are in a similar geological setting in the North-East of the Netherlands onshore region.

The main reservoir of the Groningen Gas Field is the Upper Permian/ Rotliegend Slochteren Sandstones. These sands were deposited under a dry arid climate in aeolian, fluvial or mixed conditions along the southern fringe of the Southern Permian Basin. The southernmost part of the Groningen Gas Field is located close to the southern extent of the Slochteren Formation in the area (Fig. 2) and consists of higher percentages of a conglomeratic facies, while the northern most part is close to the basin edge where increasing amounts of mudstone intercalations can be observed (de Jager and Visser, 2017, Grötsch et al., 2011). The area of the Groningen Gas field can therefore be seen as a good analogue for most of the Dutch Rotliegend gas fields (Fig. 2). The Slochteren Formation is by far the most important and prolific hydrocarbon play in the Netherlands (Doornenbal et al., 2019; Ministry of Economic Affairs and Climate Policy, Annual review 2019). The sediments of the Upper Rotliegend unconformably overlie the uplifted and eroded Upper Carboniferous and can be seen to onlap onto the Base Permian Unconformity from north to south (Grötsch et al., 2011).

Halites and anhydrites of Zechstein age form the main seal for the Groningen Gas Field as well as most of the Rotliegend gas fields in the Dutch subsurface. The thickness of Zechstein deposits controls to a large extent not only the presence of gas above or below the Zechstein but also the structural style and history as well as the fault pattern of the

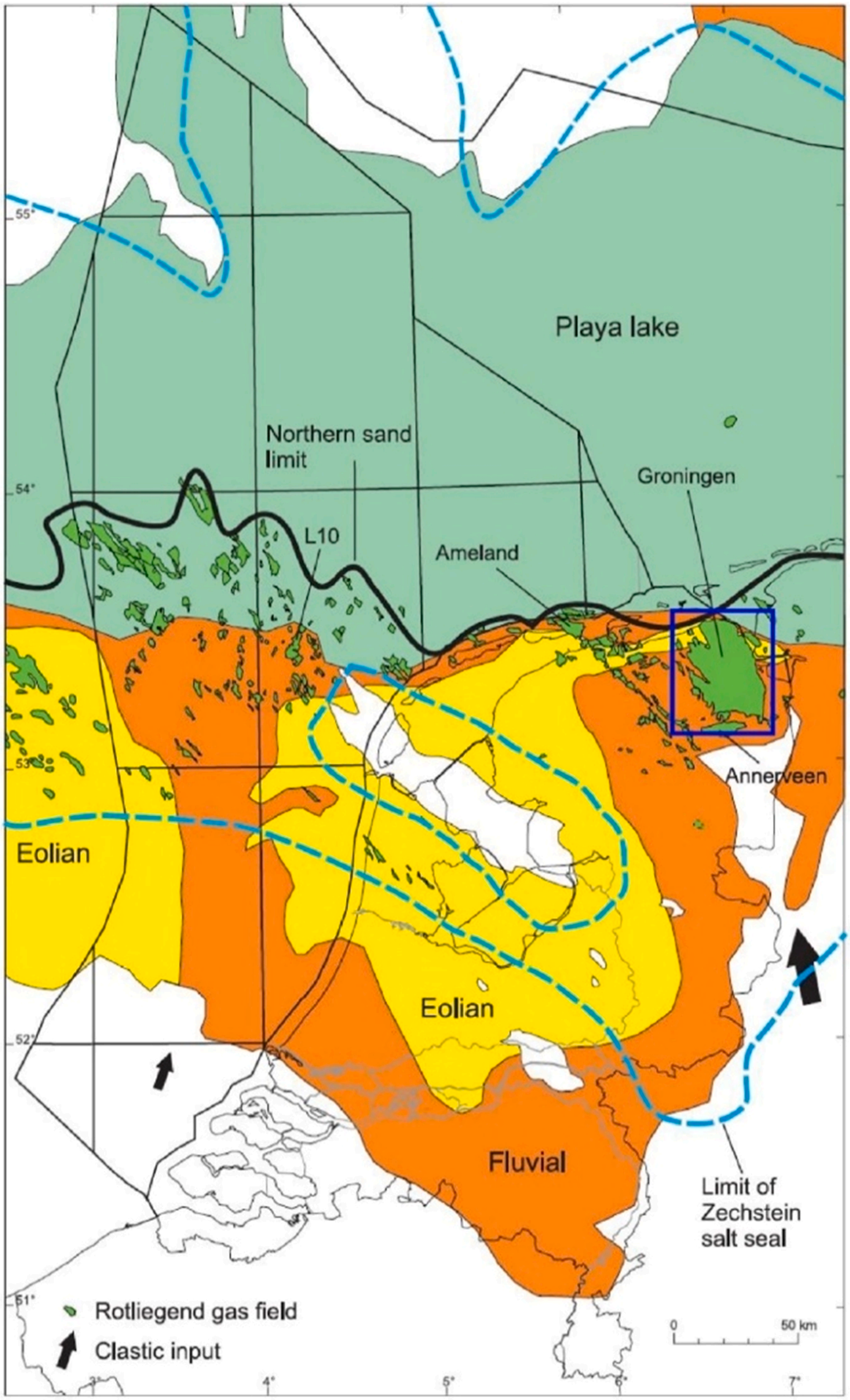

Fig. 2. Play system map of the Upper Rotliegend Slochteren Formation showing the general depositional environments, the northern extent of the Rotliegend reservoir facies (black line) as well as the southern extent of the Zechstein top seal (blue striped line; (de Jager and Geluk, 2007).

overlying strata. The Groningen area shows Zechstein thicknesses between 50 m to more than 1500 m in varying structural configurations (layer cake, salt diapirs as well as thin Zechstein due to salt withdrawal) and is therefore considered a good example for Paleozoic gas fields with Zechstein salt present.

Production of oil and gas leads to pore pressure drop in the target formation which leads to fluid flow from the surrounding formations. Over the past decades, 70 onshore gas fields and their associated wells have been abandoned in the Netherlands (Ministry of Economic Affairs and Climate Policy, Annual review 2019). More fields are still in production but will be abandoned in the near future. After production ceases, the pore pressure in and around the reservoir redistributes towards a new semi-steady state which is associated with fluid flow and potential ground motion. These processes can take place over long time frames, i.e., thousands of years (Verweij et al., 2011).

3. Model development

The numerical simulations in this work were conducted using the commercial compositional simulator CMG GEM. A two-phase (gas and liquid), two-component model was developed with a 2D axisymmetric geometry around the wellbore. The Groningen Gas Field is mainly comprised of methane with around 14 vol-% of nitrogen (Jager and Visser, 2017). However, we have not included the nitrogen content to improve runtime and for simplification. Water and methane were the only components included in the entire system. The Peng-Robinson equation of state was used to calculate gas density (Peng and Robinson, 1976), while gas viscosity was calculated using the Jossi and Stiel correlation (Jossi et al., 1962). Henry's law was used to calculate gas solubility in the aqueous phase. Harvey's correlation was used to calculate Henry's constant for methane as a function of pressure and temperature (Harvey, 1996). Aqueous phase density was calculated using the Rowe and Chou (1970) correlation, while aqueous phase viscosity was estimated using the correlation by Kestin et al. (1981). Darcy's equation was used to calculate fluid flow for each phase. Diffusive flow was calculated using Fick's law in the aqueous phase. The Wilke-Chang correlation was used to estimate molecular diffusion coefficients in the aqueous phase (Wilke and Chang, 1955). Diffusion in the gas phase and the presence of water vapor in the gas phase were ignored as their impact on the results was deemed to be negligible (Hagoort, 1988). The flow equations were discretized using an adaptive-implicit finite difference approach (Collins et al., 2003; Thomas and Thurnau, 1983; Nghiem and Li, 1989).

The modelled domain is a cylindrical wedge around the wellbore with a 10° angle. Only one grid is considered in the tangential direction, effectively making the model two dimensional. This geometry is valid assuming that the formations are homogeneous in the horizontal plane and no groundwater flow occurs in the aquifers. Therefore, potential methane plumes will be circular and uniform. The impact of groundwater flow on the plume shape and extent is not included in this study. The model extends from the base of the Slochteren Formation (the main reservoir) up to the surface for a total depth of approximately 3000 m. The outer radius of the model is 1 km, while the inner radius is the cement sheath inner radius in the well. The domain is discretized with 6150 hexahedral elements (123 × 1 × 50 in the radial, tangential and vertical direction, respectively). The grid block sizes are more refined closer to the wellbore, smallest block 0.025 m in the radial direction, while significantly larger block sizes (up to 150 m in the radial direction) are used closer to the outer boundary of the domain. The grid sizes in the vertical direction are more refined in permeable formations compared to the low-permeability clay layers. This strategy reduces the total number of grid blocks and the run-time, with minimal impact on the accuracy of the flow calculations, as most of the leakage is concentrated in high permeability pathways and formations. A version of the model with 60,000 grid blocks was also run to test the impact of grid block sizes on the results. The refined model returns comparable results as our base model.

Fig. 4 illustrates the schematic of the domain of the numerical model. The grid blocks at the left corner of the cylindrical wedge represent the cement sheath. The cement sheath connects all the formations from the reservoir all the way to the atmosphere. The fluid leakage along the well is assumed to occur through the cement sheath. The casing on the left of the cement sheath is assumed to be a no-flow boundary. A no-flow boundary is also assumed at the base of the reservoir. The outer boundary on the right side of the wedge is assumed to be at a constant pressure. The radius of the wedge is large enough that the impact of gas leakage over 100 years does not reach the boundary in any of the simulations in this work. The top of the model is assumed to be at a constant pressure representing the atmosphere.

The simplified stratigraphy of the region is reflected in the model. The detailed stratigraphy was obtained from the NLOG database (e.g., well ZWD-01, nlog.nl – retrieved Jan. 2021). We simplified the stratigraphy by removing thin and insignificant (in the context of fluid flow) layers and lumping several formations that likely have similar flow properties. Table 1 presents the simplified stratigraphy represented by the model in Fig. 4.

Boxtel Formation sits at the top of the model, which is a 20 m thick unconfined freshwater aquifer in the region of study. Peelo Formation is immediately under the Boxtel Formation and is comprised of an aquitard and a confined freshwater aquifer, extending down to 204 m depth. The Breda Formation underlies the Peelo Formation and could be a source of free gas due to the presence of thin coal layers (TNO-GDN, 2022). Some of the sealing formations were grouped together as Clay 1, Clay 2, and Clay 3. The Brussels Sand Member is a sand formation saturated with brine. The Ommelanden formation is a thick chalk layer that is permeable in the upper zone and impermeable in the bottom portion. Organic-rich Claystone is a collection of organic-rich marl and clay members dispersed with coal that could be a source of free gas. In this work, only the Organic-rich Claystone was considered to be a shallow source of gas. The impact of gas presence in Breda Formation was not included for brevity. The caprock is 800 m thick, over-pressured and is comprised of marl, claystone, and evaporites. The Slochteren Formation is the main reservoir currently at 7 MPa pressure, with a planned abandonment pressure of 6 MPa (SGS Horizon BV, 2016; van Elk et al. 2021). The virgin reservoir pressure was 34.5 MPa. A temperature gradient of 31.3 °C/km with a surface temperature of 10.1 °C was used to estimate the temperature profile (Bonté et al., 2012; Békési et al., 2020). Water salinity in the freshwater aquifers is expected to be close to zero. Salinity increases with depth to a maximum of 280,000 mg/l in the reservoir (Burkitov et al., 2016), however for simplicity we assumed a constant average salinity of 100,000 mg/l for the entire model (except the freshwater aquifers). The cement sheath was assumed to be debonded from the casing along the entire length of the well. An average permeability was assigned to the entire cement sheath. Two damage levels were considered for the cement sheath. Based on the recent studies in the literature, an average cement sheath permeability of 100 mD is at the top of the range of the measured or inferred values in wells (Gasda et al., 2013; Kang et al., 2015; Tao and Bryant, 2014; Moghadam et al., 2020, 2022). Therefore, an extremely damaged cement sheath was assumed to have a permeability of 100 mD. A mildly damaged cement sheath was assigned an average permeability of 1 mD.

The following modified Brooks-Corey relationships were used to calculate gas and water relative permeability terms (Fanchi, 2018):

$$k_{rg} = k_{rg}^{max}\left(\frac{s_g - s_{gc}}{1 - s_{wc} - s_{gc}}\right)^{n_g} \tag{1}$$

$$k_{rw} = k_{rw}^{max}\left(\frac{s_w - s_{wc}}{1 - s_{wc}}\right)^{n_w} \tag{2}$$

where, k_{rg} and k_{rw} are gas and water relative permeabilities. k_{rg}^{max} and k_{rw}^{max} are the maximum relative permeability values for gas and water, respectively. s_g and s_w refer to gas and water saturation. s_{gc} and s_{wc} are the critical gas and irreducible water saturations, respectively. n_g and n_w are empirical exponents. Critical gas saturation is the minimum gas saturation needed for the gas to flow as a bulk phase.

Capillary pressure curves were estimated using the formulation proposed by Brooks and Corey (1964), presented in Eq. (3):

$$P_c = P_e\left(\frac{s_w - s_{wr}}{1 - s_{wr} - s_{gr}}\right)^{\frac{-1}{\lambda}} \tag{3}$$

Table 1
Summary of the stratigraphy and petrophysical properties at the ZWD-01 well location.

Summarized Stratigraphy	Description	Formation Top (m)	Thickness (m)	Pressure Condition	Porosity	Permeability[1] (mD)	Data Sources
Boxtel Aquifer	Sand	0	19	Normally pressured	0.4	4500	Porosity and permeability: ThermoGIS.nl
Peelo Aquitard	Clay	19	22	Normally pressured	0.5	0.1	Full stratigraphy: NLOG.nl, well name ZWD-01
Peelo Aquifer	Sand	41	163	Normally pressured	0.4	20,000	Pressure: PSNS database (TNO, 2015)
Breda Formation	Sandy clay	204	91	Normally pressured	0.5	1	
Clay 1	Clay	295	142	Normally pressured	0.35	0.1	
Brussel Member	Sand	437	145	Normally pressured	0.34	500	
Clay 2	Clay	582	324	Normally pressured	0.32	0.1	
Ommelanden - top	Chalk	906	494	Normally pressured	0.33	100	
Ommelanden - bottom	Chalk	1400	361	Normally pressured	0.1	0.5	
Clay 3	Clay	1761	110	Normally pressured	0.21	0.01	
Organic-rich Claystone	Clay (potential gas source)	1871	173	Normally pressured	0.14	5	
Caprock	Marl, claystone, evaporites	2043	829	Over-pressured (11 MPa excess)	0.03	0.0001	
Slochteren Formation	Sand (target reservoir)	2872	81	Depleted (6 MPa)	0.15	32	

[1] The ratio of vertical to horizontal permeability was assumed to be 0.1 everywhere, except the freshwater aquifers where a value of 0.5 was used.

where, P_c is the gas-water capillary pressure, P_e is the capillary entry pressure, and λ is the pore size distribution index. s_{wr} and s_{gr} refer to the residual (irreducible) water and gas saturations, respectively.

For the leakage conditions modelled in this work, gas is expected to escape the reservoir or other sources, travel upwards through the cement sheath to invade shallower brine saturated formations. This indicates drainage to be the primary invasion process, as gas enters various water saturated formations. Therefore, the relative permeability and capillary pressure terms used for the model were selected to be suitable for the drainage process. For the drainage process, k_{rw}^{max} can be set to 1 (Li and Horne, 2006; Shi et al., 2018). To reduce the number of parameters, we assumed that the critical and residual gas saturations were equal. The irreducible water saturation was estimated using the relationship proposed by Lopez et al. (2013) based on formation permeability. Capillary entry pressures were estimated using the correlation proposed by Huet et al. (2005), converted to a gas-water system. The Leverett J-function was used to scale the capillary entry pressure when formation permeability or porosity was changed for a simulation case. Critical gas saturation was assumed to be 1% for the high permeability aquifers increasing to 25% for the caprock. The relative permeability exponents were assumed to be 5 for the caprock, decreasing with an increase in formation permeability. λ was assumed to 0.75 for the caprock, increasing to 3 for the high permeability aquifers. The leakage pathway along the cement was assumed to be in the form of a debonded interface. Therefore, the flow properties of the cement sheath were assumed to be similar to a fracture, i.e., a low capillary entry pressure and linear relative permeability curves ($n_g = n_w = 1$). The petrophysical and multiphase flow properties of the main reservoir were taken from the models developed by NAM (Nederlandse Aardolie Maatschappij) which operates the field (Burkitov et al., 2016). In total, six rock types were considered to cover the entire domain of study. Each modelled formation in Table 1 is assigned to a rock type. Table 2 provides a summary of the parameters and the formations assigned to each rock type.

Based on the stratigraphy and the gas shows during drilling (www.dinoloket.nl, EBN Gas Shows database, retrieved Jan. 2021), the Organic-rich Claystone (ORC) was identified as a potential source of free gas in the system (Fig. 3), in addition to the Slochteren Formation (main/target reservoir). The gas saturation in the reservoir is approximately 80% (SGS Horizon BV, 2016). However, the saturation is uncertain in the ORC. We considered gas saturations of 10% and 60% to investigate the impact of the uncertainty on leakage. The permeability of the ORC was also changed by an order of magnitude to quantify its impact.

Table 3 provides a description of all the simulation cases in this study. Cases 1 to 7 consider the main reservoir to be the only source of free gas. Cases 8 to 17 assume that both the main reservoir and the Organic-rich Claystone contain free gas.

Table 2
Summary of the input parameters for 6 rock types considered in this study.

Rock type	Formations	k_{rg}^{max}	n_w, n_g	s_{gc}	s_{wc}	λ	P_e (kPa)
1	Slochteren Formation (reservoir)	0.86	4	0.15	0.16	1.0	100
2	Caprock, Clay 3	0.20	6	0.25	0.65	0.5	3043
3	Clay 1, Clay 2, Peelo aquitard, Ommelanden – bottom	0.60	5	0.20	0.40	0.75	593
4	Organic-rich Claystone, Brussel Member, Ommelanden - top, Breda Formation	0.75	3	0.10	0.20	1.5	22
5	Peelo aquifer, Boxtel aquifer	1.0	2	0.01	0.10	3.0	2
6	Microannulus (cement sheath)	1.0	1	0.05	0.10	3.0	1

The simulation domain was initialized assuming all the formations were fully saturated with water, except the one or two formations that contained free gas (depending on the simulation case). The thickness of the gas cap in the ORC was assumed to be 15 m, in cases 8 to 17. The water-gas contact in the reservoir was assumed to be below the base of the model (only gas cap is modelled in the reservoir). The initial pressure in the entire model was hydrostatic, except the caprock and the reservoir. The caprock in this field is over pressured by approximately 11 MPa (TNO, 2015). The reservoir was initialized at its expected abandonment pressure of 6 MPa, which is likely to be reached in 2023. Water was assumed to be fully saturated with dissolved methane in all the formations, except the freshwater aquifers (Boxtel and Peelo). All simulations were run for 100 years after the start of gas leakage.

4. Results

In this section, we present the results of the gas leakage modeling. The results are organized according to the main source of gas considered. Initially, only the depleted reservoir is assumed to contain free gas. Subsequently, leakage values assuming both the reservoir and ORC as sources of free gas are presented. All leakage rates in the following

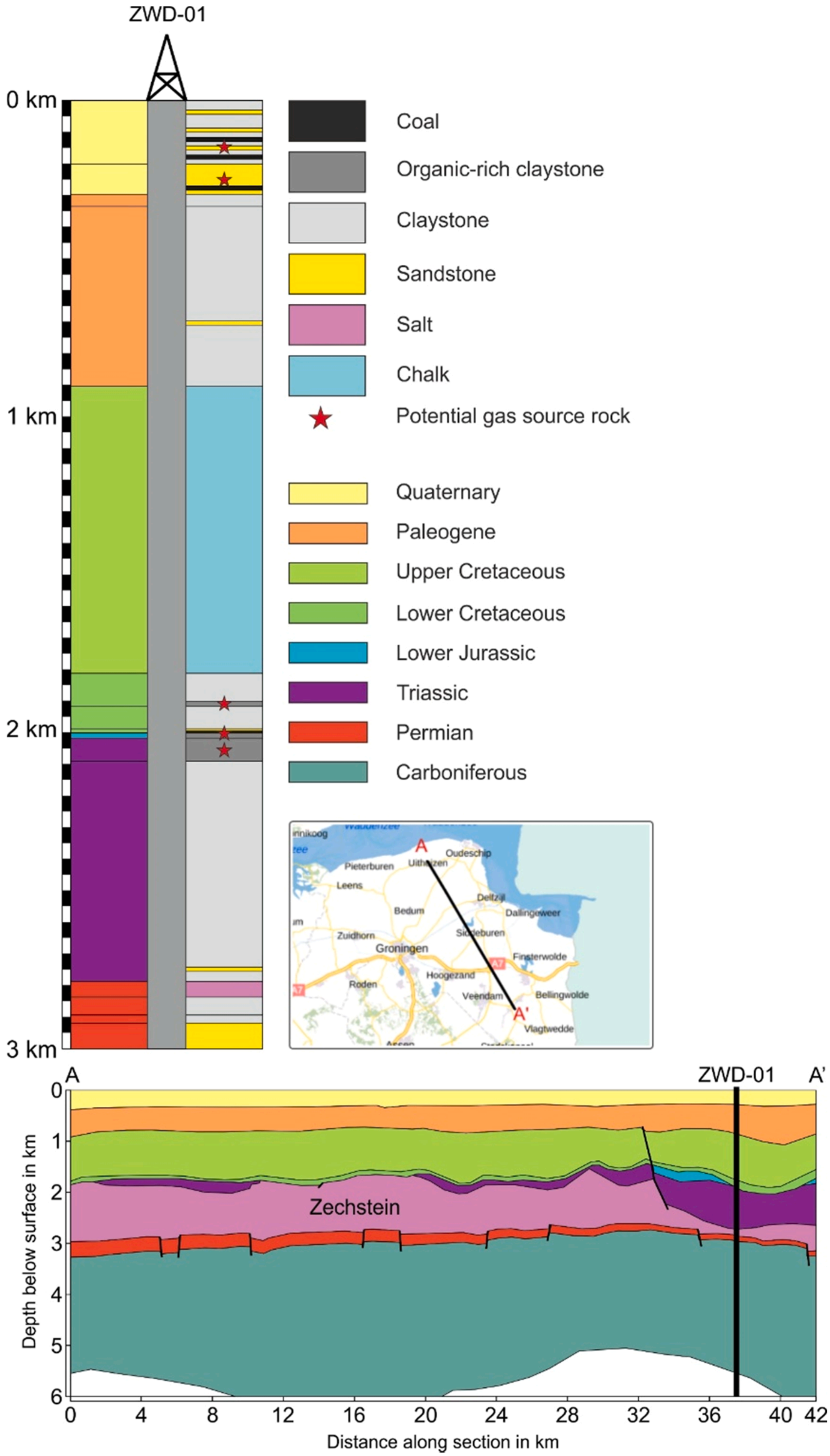

Fig. 3. 2D Cross section through the Groningen Gas Field from NNW to SSE, crossing well ZWD-01 showing the main structures and formations in the area (redrawn from www.dinoloket.nl).

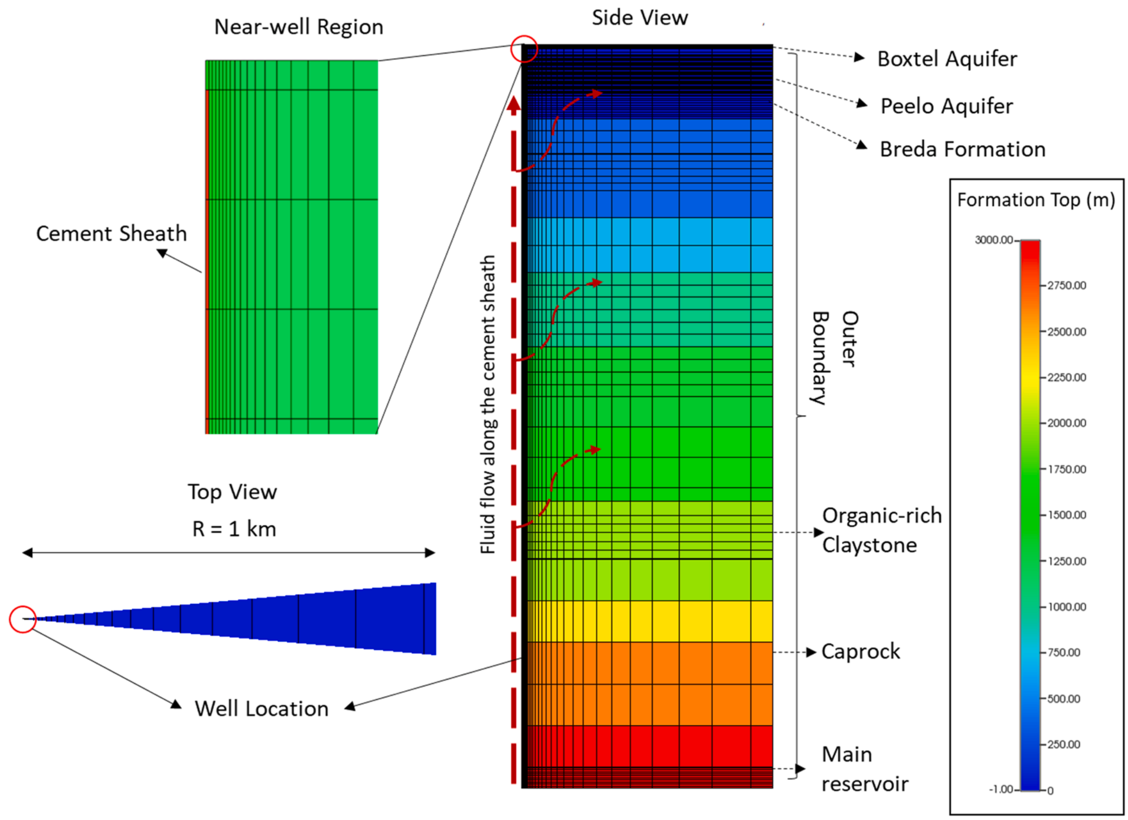

Fig. 4. A schematic of the domain of the numerical study. The near-well region is magnified on the top left (color scheme correlates with permeability – not scaled to the color bar). The bottom left section shows the top view of the cylindrical wedge (top of the model) with a radius of 1 km (color corresponds to the formation top represented by the color bar). The well (cement sheath) is located at the left corner of the wedge and connects all the formations. The image in the center illustrates the side view of the domain. The stratigraphy in the region is summarized and represented in the model from the base of the reservoir at the depth of 2950 m to the surface.

Table 3
Details of the simulation cases considered in this work. "ORC" refers to the Organic-rich Claystone. For each case, the values of gas saturation, pressure, and permeability of each gas source are presented in the same order as the gas source. "NP" indicates "normally-pressured", and "OP" means Over-pressured".

Case number	Gas source	Gas saturation at each source	Pressure at each source (kPa)	Permeability of each source (mD)	Cement sheath permeability (mD)
1	Reservoir	0.8	6000	32	1
2	Reservoir	0.8	6000	32	100
3	No source of free gas	–	6000	32	100
4	Reservoir (hydrostatic seal)	0.8	34,500	32	100
5	Reservoir (hydrostatic seal)	0.8	34,500	32	1
6	Reservoir (no-flow seal)	0.8	34,500	32	100
7	Reservoir (no-flow seal)	0.8	34,500	32	1
8	Reservoir, ORC	0.8, 0.1	6000, NP	32, 5	1
9	Reservoir, ORC	0.8, 0.1	6000, NP	32, 5	100
10	Reservoir, ORC	0.8, 0.6	6000, NP	32, 5	1
11	Reservoir, ORC	0.8, 0.6	6000, NP	32, 5	100
12	Reservoir, ORC	0.8, 0.6	6000, NP	32, 50	1
13	Reservoir, ORC	0.8, 0.6	6000, NP	32, 50	100
14	Reservoir, ORC	0.8, 0.6	6000, 10% OP	32, 5	1
15	Reservoir, ORC	0.8, 0.6	6000, 10% OP	32, 5	100
16	Reservoir, ORC	0.8, 0.6	6000, 10% OP	32, 50	1
17	Reservoir, ORC	0.8, 0.6	6000, 10% OP	32, 50	100

sections have been multiplied by 36 to convert the rate through the 10° wedge around the well to the equivalent 3D model (360°). A preliminary version of the results, along with an assessment of long-term re-pressurization of the Groningen field is reported by TNO and Deltares (2022).

4.1. *Reservoir leakage*

4.1.1. *Depleted reservoir*

The simulation cases 1 to 7 assume the depleted reservoir to be the only source of gas. Cases 1 and 2 consider the gas reservoir to be depleted at 6 MPa pore pressure. Fig. 5 presents the rate of influx of water and methane in the reservoir over 100 years, for cases 1 and 2. The

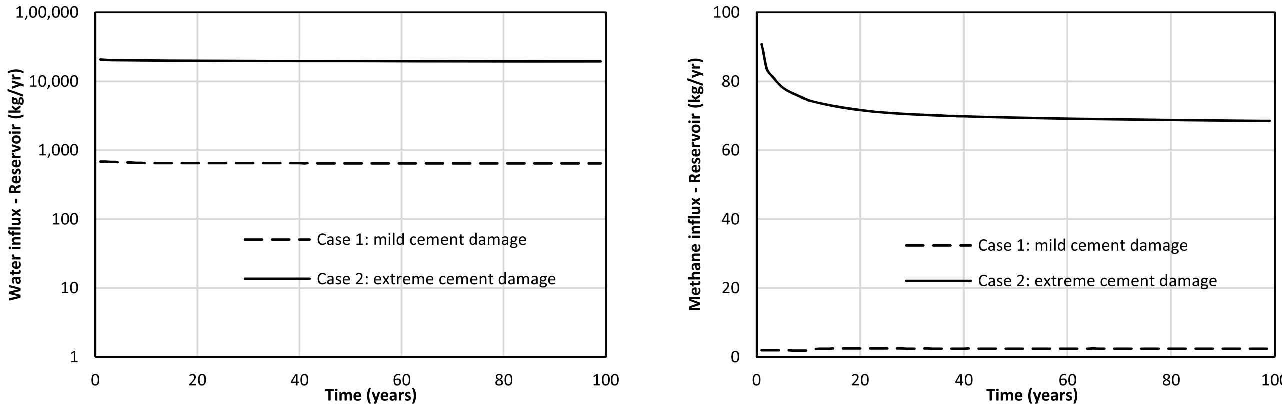

Fig. 5. Water and methane rate of influx in the depleted reservoir over 100 years.

results indicate positive influxes for both methane and water, signifying fluid flow into the reservoir over time. Mild cement damage (average cement sheath permeability of 1 mD) leads to a significantly smaller influx rate for both methane and water (case 1). The mild damage case shows a water influx of 600 kg/yr (equivalent to 0.0016 m^3/d), while the extremely damaged cement (100 mD) leads to water influx of 20,000 kg/yr (equivalent to 0.055 m^3/d) into the reservoir. Methane also flows into the reservoir, albeit at a much lower rate. Methane does not leak out of the reservoir due to the low pressure compared to the overlying formations. The source of the observed methane influx is the dissolved methane in the water invading the reservoir through the microannulus. Water is assumed to be fully saturated with methane in the entire system, except the shallow aquifers (Peelo and Boxtel). Methane enters the reservoir at a rate of 2.4 kg/yr for the mildly damaged cement, and an initial rate of 90 kg/yr for the extremely damaged cement (eventually reaching 70 kg/yr after 40 years).

Fig. 6 presents the combined rate of methane leakage into the aquifers and atmosphere for cases 1 to 3. Case 3 assumes that no free gas exists in the entire system, not even in the reservoir. This hypothetical scenario aims to set a baseline to determine the relative impact of free gas in the system. Mild cement damage causes negligible methane leakage into the atmosphere and aquifer system. Extreme cement damage leads to a steady-state leakage rate of approximately 15 kg/yr. The methane leakage in case 3 (with no free gas) is similar to case 2 (both with an extremely damaged cement sheath). Therefore, the leakage rate observed in cases 1 to 3 is not due to convective flow of the free gas from the reservoir. In these cases, leakage occurs due to diffusive and convective flow of the dissolved methane in the underlying formations. The order of magnitude of the rates illustrated in Fig. 6 is very small compared to the scale of the system under study. The leakage rate for case 1 (mild damage) is close to zero.

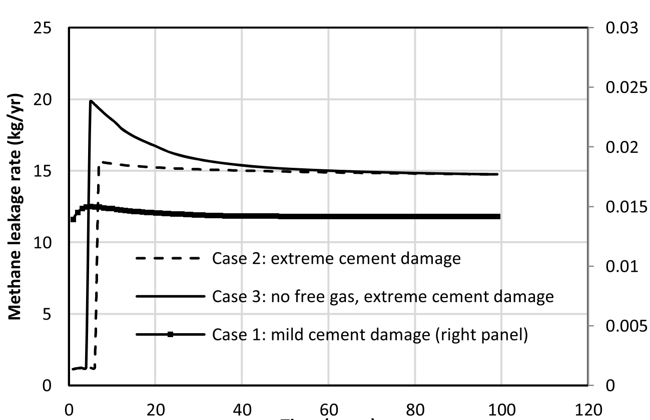

Fig. 6. Combined rate of leakage into the aquifers and atmosphere for cases 1 to 3.

Fig. 7 illustrates the extent of the dissolved methane plume in the Peelo and Boxtel aquifers after 100 years, for cases 1 to 3. Dissolved methane content above 1 mg/l is depicted in red and used loosely to define the extent of the plume. Case 1 (mild cement damage) shows a small methane plume at the base of the Peelo formation. Case 2 and 3 show a dissolved plume that extends approximately 20 m away from the well after 100 years (not considering the impact of groundwater flow). No free gas is observed in the Peelo and Boxtel aquifers after 100 years, for cases 1 to 3.

4.1.2. *Reservoir at virgin pressure*

Cases 4 and 5 assume that the reservoir is at its initial pressure of 34.5 MPa. The aim is to investigate potential gas leakage rates for wells drilled in virgin reservoir blocks. Fig. 8 presents the methane leakage rate values for each case, in the atmosphere and into the Peelo Formation. The extremely damaged cement sheath in case 4 shows a steady-state methane leakage rate of 800 kg/yr into the atmosphere. The leakage rate in the Peelo Formation reaches a high of 60 kg/yr for the same case. The mild cement damage shows a steady-state leakage rate of 7 kg/yr and 14 kg/yr into the atmosphere and Peelo Formation, respectively. The Boxtel Formation is an unconfined aquifer in the area under study. Methane did not significantly accumulate in the Boxtel Formation in any of the simulations conducted in this work, as the leaked methane into the formation eventually flow up into the atmosphere. Therefore, only the leakage into the atmosphere and the Peelo aquifer is discussed.

In cases 4 and 5, the caprock fluid pressure acts as a barrier against leakage in the microannulus. In some cases, such as in salt formations, no fluid pressure exists in the caprock. Cases 6 and 7 consider the caprock as a no-flow boundary. This is done by disabling the blocks representing the caprock. Therefore, the reservoir is connected to the overlying formations only through the cement sheath. Fig. 9 presents the rate of methane leakage into the atmosphere and Peelo aquifer for cases 6 and 7. According to Fig. 9, the extremely damaged cement sheath leads to a leakage rate of 800 kg/yr and 3300 kg/yr in the atmosphere and the Peelo aquifer, respectively. Mild cement damage leads to relatively negligible leak rates of 7 kg/yr and 23 kg/yr in the atmosphere and Peelo aquifer, respectively. We define "negligible leak" loosely based on the average emission of a single dairy cow which is estimated to be 100 kg/yr.

The gas composition in the main reservoir (Slochteren Formation) was assumed to be comprised of only methane. However, the Groningen Field contains approximately 14 vol-% of nitrogen. This simplification does not alter the main processes but means that for this particular case, the methane leakage from the Groningen reservoir is overestimated. However, shallower sources of gas are likely to have a higher methane

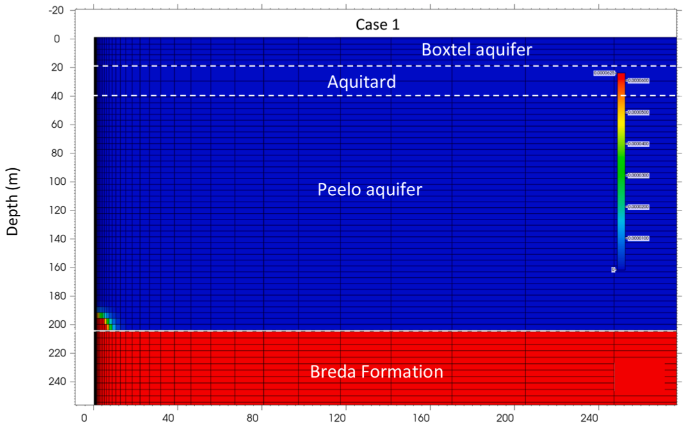

Fig. 7. The extent of the dissolved methane plume in the Peelo and Boxtel aquifers after 100 years for cases 1 to 3. The cement sheath is on the left of the domain. The red areas indicate a dissolved methane content above 1 mg/l. The scale on the color bar ranges between 0 and 0.0000625 gmol/kg.

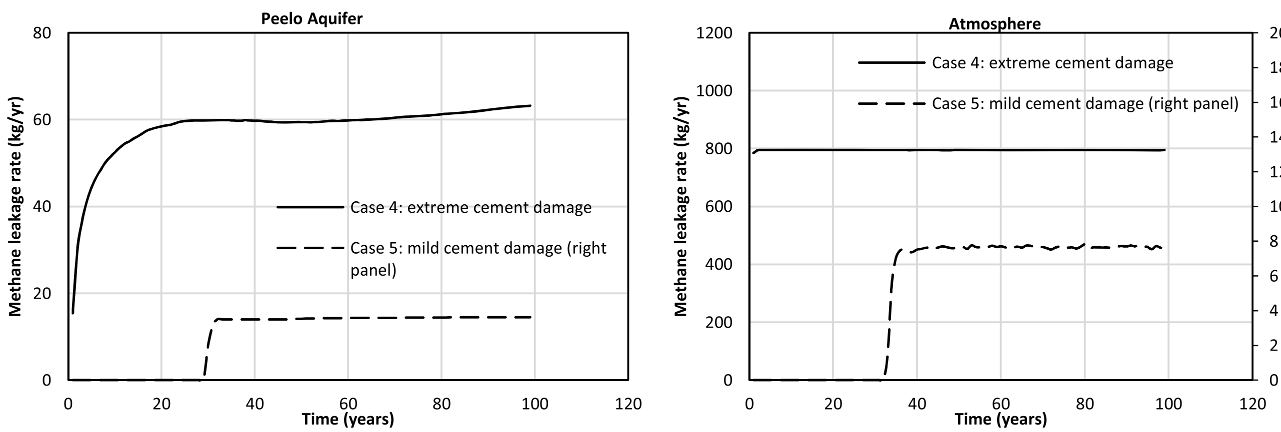

Fig. 8. Rate of leakage into the aquifer and atmosphere for cases 4 and 5 (reservoir at virgin pressure).

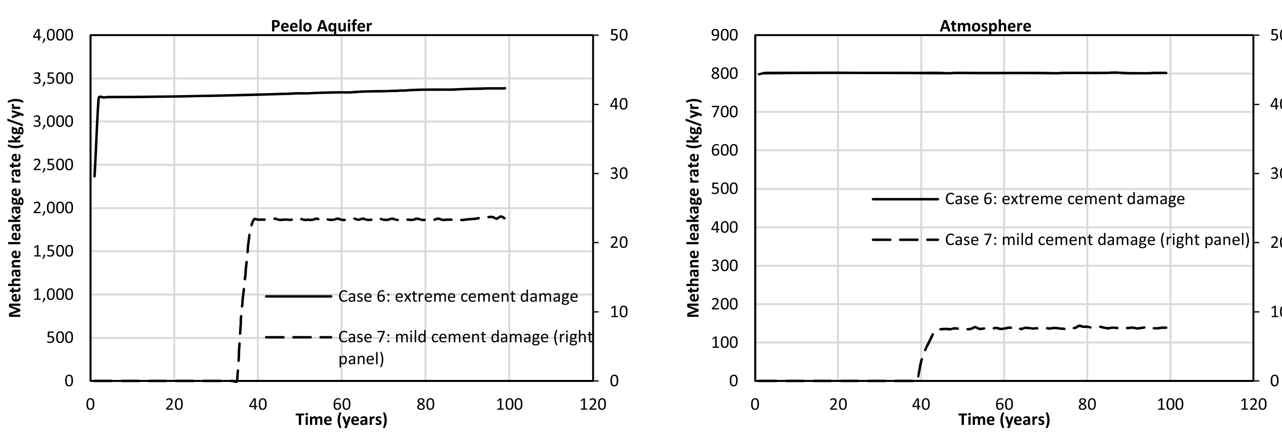

Fig. 9. Rate of leakage into the Peelo aquifer and atmosphere for cases 6 and 7 (reservoir at virgin pressure and no-flow boundary in the caprock).

content.

Fig. 10 illustrates the extent of the free methane plume in the shallow aquifers on the left, and the extent of the dissolved methane plume on the right, for case 6 after 100 years (assuming no groundwater flow). The reach of the free methane plume is demonstrated using water saturation. The free gas plume reaches as far as 350 m away from the wellbore after 100 years. Gas saturation in the vicinity of the wellbore increases to 25%. Free gas will also be stored in the Breda Formation and the Brussels Sand Member. The dissolved methane front reaches as far as 450 m away from the wellbore after 100 years. Case 7 which represents a mildly damaged cement sheath also shows a small amount of free gas in the Peelo formation, reaching a max saturation of 5% near the wellbore with free gas plume extending to nearly 20 m away from the well.

4.2. *Organic-rich claystone (ORC)*

Cases 8 to 17 consider both the depleted reservoir and the Organic-rich Claystone (ORC) to be sources of free gas. The reservoir is set to its abandonment pressure of 6 MPa for all the ORC related cases (8 to 17). Gas saturation in the ORC is not known. Cases 8 and 9 assume a gas

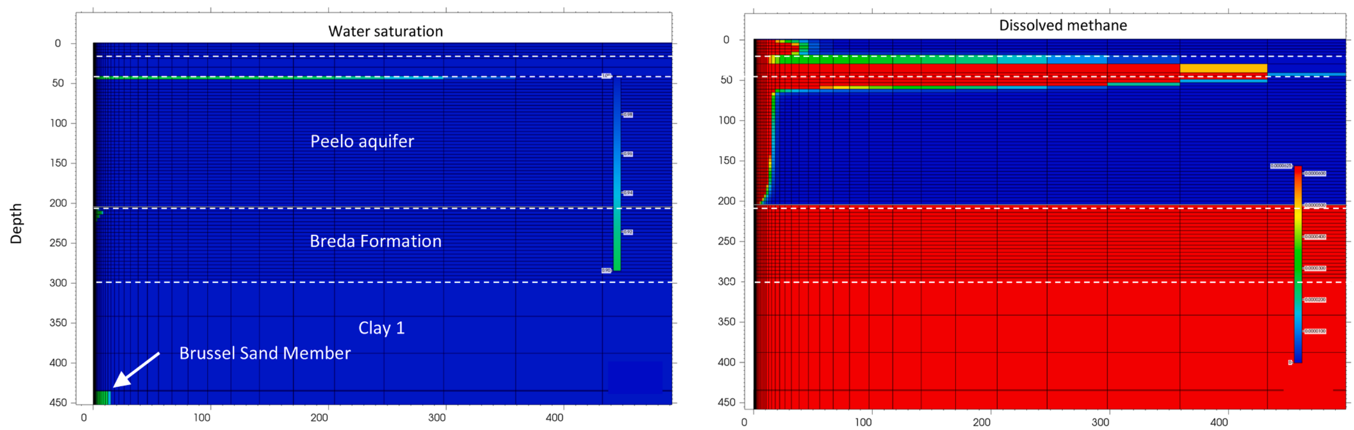

Fig. 10. The extent of the free methane plume on the left and the dissolved methane on the right, in the shallow aquifers after 100 years for case 6. The water saturation in the color bar ranges between 0.9 (light green) and 1.0 (dark blue). The color bar representing the dissolved methane content ranges between 0 and 0.0000625 gmol/kg (equivalent to 1 mg/l). The dashed lines distinguish different formations.

saturation of 10% in the ORC. Critical gas saturation in the ORC is also assumed to be 10%. Fig. 11 indicates the combined methane leakage rate into the aquifer-atmosphere system. Negligible leakage is observed for a mildly damaged cement sheath. Case 9 represents an extremely damaged cement and shows a leakage rate of approximately 15 kg/yr, similar to cases 2 and 3 in Fig. 6. This indicates that if the gas saturation in the ORC is at or below the critical gas saturation, it will not contribute to leakage significantly.

Cases 10 and 11 assume a gas saturation of 60% for the ORC, and they represent mild and extreme cement damage scenarios, respectively. Fig. 12 shows the methane leakage rate in the atmosphere and the Peelo aquifer for each case. The mild cement damage shows minimal leakage into the atmosphere and the Peelo aquifer. The extremely damaged cement sheath leads to a leakage rate between 3300 and 3500 kg/yr for the Peelo aquifer, and approximately 800 kg/yr for the atmosphere. Similar to cases 6 and 7, free gas is stored in the Peelo aquifer and free and dissolved methane plumes reach as far as 350 and 450 m away from the wellbore, respectively.

Similar to the gas saturation, the permeability and the pressure of the ORC is relatively uncertain. Cases 12 to 17 assume a combination of higher permeability, by a factor of ten from 5 to 50 mD, and a 10% overpressure in the ORC. Fig. 13 presents the methane leakage rate in the atmosphere and the Peelo aquifer for cases 11 and 17, both of which consider an extremely damaged cement sheath. Case 17 assumes a permeability of 50 mD and a 10% overpressure in the ORC. According to Fig. 13, the resulting leakage is identical to case 11 which assumes a 5 mD permeability and hydrostatic pressure. This is an indication that for

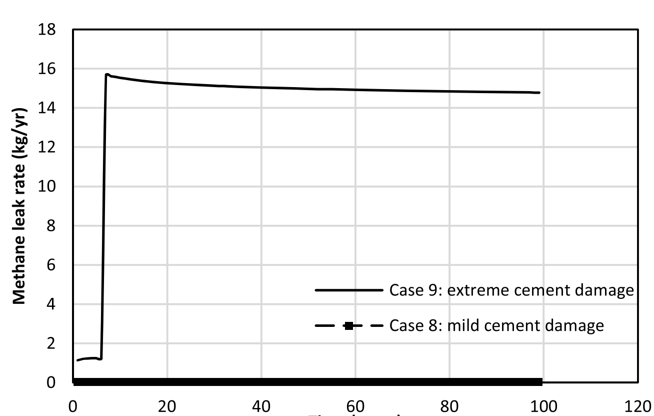

Fig. 11. Methane leakage rate into the combined aquifer and atmosphere system assuming 10% gas saturation in ORC (cases 8 and 9).

the particular system in this study, the cement permeability controls the leak rate into the atmosphere and aquifer system.

5. Discussion

5.1. Reservoir re-pressurization

The results of case 2 presented in Fig. 5 indicate a positive influx of water and methane into the depleted reservoir after abandonment. The fluid influx is due to the low pressure in the reservoir compared to the overlying formations which creates a large downward pressure gradient. The water influx is expected to increase the pressure and water saturation near the wellbore in the reservoir. Fig. 14 shows the change in water pressure and saturation near the wellbore after 100 years, for case 2 (extremely damaged cement). The results show that pressure increases from 6000 to 6500 kPa after 100 years due to water flow into the reservoir. The water saturation increases from 0.2 to 0.45. The pressure increase will be transmitted as far as 100 m away from the well. The relatively small pressure increase (compared to the initial formation pressure) suggests that water leakage is not high enough to cause significant re-pressurization in the reservoir. The results shown in Figs. 5 and 14 indicate that a severely depleted reservoir is not a likely source of gas leaks, as long as the pressure remains low.

For the Groningen field, the connected aquifers could eventually pressurize the gas. However, it has been shown that the gas pressurization in the Groningen field will be minimal after 500 years due to the high compressibility of gas and the relatively small size and low permeability of the connected aquifers (TNO and Deltares, 2022). Smaller gas fields with strong pressure support from nearby aquifers could experience pressurization and eventually start to leak. The risk of re-pressurization and leakage should be assessed for these reservoirs.

5.2. Impact of buoyancy

The claim that under-pressured gas will not flow upwards through the microannulus may seem counter intuitive. Due to its lower density, it is intuitive to think that gas when placed against water in a permeable path should flow upwards. However, this can only occur if the buoyancy is sufficient to overcome the pressure difference between the under-pressured gas in the reservoir and the water in the damaged cement sheath (i.e., a microannulus) and overlying formations. We can support this claim conceptually in the following.

Eq. (4) can be used to calculate fluid flow in the microannulus considering the density effects (Moghadam et al., 2022):

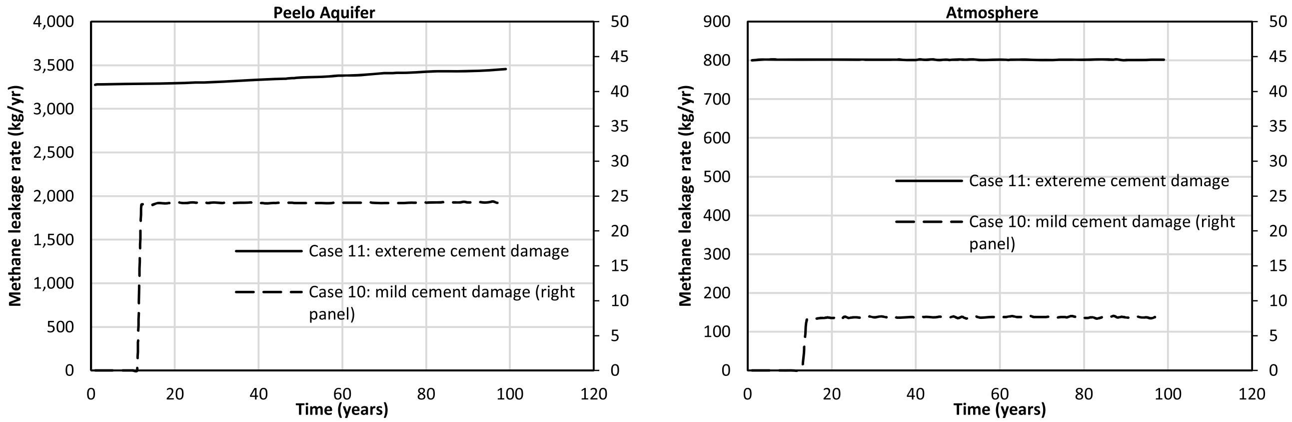

Fig. 12. Rate of leakage into the Peelo aquifer and atmosphere for cases 10 and 11 (60% gas saturation in the ORC).

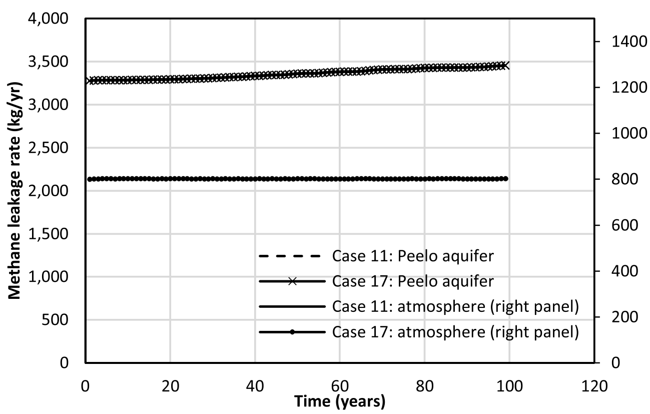

Fig. 13. Methane leakage rate into the combined aquifer and atmosphere system assuming 60% gas saturation in ORC (case 11: hydrostatic pressure and permeability is 5 mD, and case 17: 10% overpressure and permeability is 50 mD).

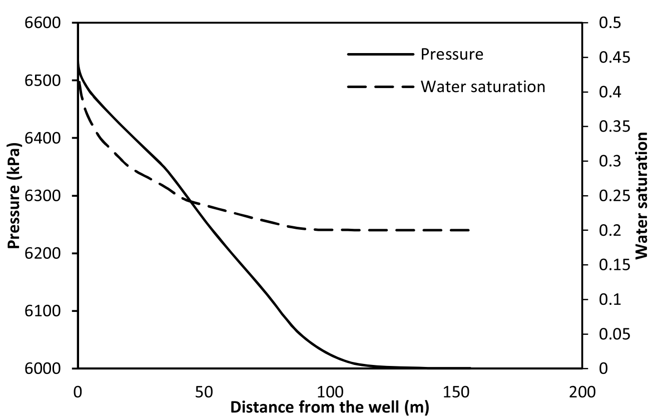

Fig. 14. Gas pressure and water saturation versus distance from the wellbore after 100 years for an extremely damaged cement (case 2).

$$\dot{m} = \frac{\rho(P,T)}{\mu(P,T)} \times \frac{\pi R w^3}{6} \frac{\partial(P-\rho g z)}{\partial z} \tag{4}$$

where $\dot{m}$ is the mass flow rate of gas, ρ and μ are gas density and viscosity, R is the casing outer radius, w is the hydraulic aperture of the microannulus, P is the gas pressure, and z represents depth. This is a form of the Darcy equation suitable for fracture flow, where the permeability is replaced by its equivalent according to the cubic law. The term $\Phi = (P - \rho g z)$ is the flow potential and is a representation of buoyancy flow (assuming z is positive in downward direction). In order for flow to occur, there must be a flow potential gradient present between two points along a microannulus.

Fig. 15 presents a conceptual model of a gas reservoir (permeable formation) that underlies a caprock and is connected to a microannulus. The microannulus is a crack along the outside of the casing. The cement sheath is typically 2 cm thick and can contain disking cracks due to shrinkage. Therefore, it can be assumed that, barring any flow, at each depth the initial pressure of the microannulus is in equilibrium with the formation and is likely filled with brine above the gas-filled reservoir. The capillary pressure (Pc) for a crack is typically in the range of a few kPa (Wang et al., 2017; Wang and Cardenas, 2018) which is orders of magnitude less than the pressures involved in this study. The capillary pressure inside the reservoir rock is higher than the capillary pressure microannulus. However, the formation capillary pressure is still small as the reservoir is a permeable sandstone (expected Pc in the range of a few hundreds of kPa). Therefore, the impact of the capillary pressure gradient for gas invasion in the microannulus is small.

Let us consider two depths of interest, one at the top of the reservoir and another at the top of the caprock. Assuming hydrostatic pressure for water in the entire system, we have:

$$P_{w,1} = \rho_w g h_1, \quad P_{w,2} = \rho_w g h_2 \tag{5}$$

This leads to $\Phi_{w,1} = \Phi_{w,2} = 0$, which indicates a zero flow potential gradient for water across the caprock. Therefore, no flow will occur in a system where no density difference exists and pressures are hydrostatic.

The initial pressure of the gas in the reservoir depends on the pressure at the depth of the gas-water contact (h_{GWC}) and the height of the gas column above this depth. The depth of the gas-water contact (h_{GWC}) is defined as the depth at which $P_g = P_w = \rho_w g h_{GWC}$ (sometimes also referred to as Free Water Level). The Φ_g (gas flow potential)at the top of the reservoir can be calculated using the gas density ρ_g for the

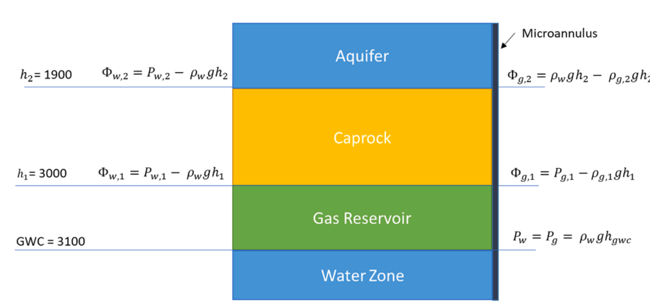

Fig. 15. Conceptual model to assess the impact of buoyancy in gas/ water systems.

gravity term. The flow potential of the gas at h_1 is:

$$\Phi_{g,\,1} = P_g - \rho_g g h_1 = \rho_w g h_{GWC} - \rho_g g(h_{GWC} - h_1) - \rho_g g h_1 = \rho_w g h_{GWC} - \rho_g g h_{GWC} \tag{6}$$

$\Phi_{g,\,1}$according to Eq. (6) is non-zero. This shows that due to buoyancy, gas will flow upwards if no caprock exists. The presence of the caprock with a high capillary entry pressure prevents flow. However, if a microannulus exists along the length of the well, gas has a path with a negligible capillary entry pressure to flow upwards.

In case of a depleted reservoir, the gas flow potential in the reservoir will decrease. To assess whether the gas will flow upwards in the presence of a microannulus, $\Delta\Phi_g$ (the flow potential difference) between the top of the reservoir (h_1) and the base of the aquifer above the caprock (h_2) should be calculated. The key assumption is the pressure state in the microannulus. The microannulus is initially filled with water. The caprock has a low permeability and likely will not maintain a constant water pressure over time in the microannulus (water will flow into the reservoir and gas will further depressurize water over time). However, it is plausible that at a certain depth an aquifer with sufficient permeability exists that can maintain a constant pressure in the microannulus (maintain a water column). The microannulus has an aperture between 20 and 200 μm (Moghadam et al., 2022; Orlic et al., 2018) and therefore small volumes of water can be sufficient to provide pressure support. As the reservoir is depleted, Φ_w (the flow potential of the water) in the reservoir will become negative and water will flow down through the microannulus into the reservoir. For Φ_g (the flow potential of the gas), we need to make an assumption about the pressure in the microannulus at the depth of h_2. If the microannulus has no contact with permeable aquifers and is gas filled, the pressure would be based on the reservoir pressure and for example 6 MPa would still be higher than the gravity term, because of the very low density of methane at low pressures (~0.8 kg/m^3 for 0.1 MPa; ~35–40 kg/m^3 at 6 MPa). This means that without pressure support from an aquifer, a gas formation can leak until its pressure drops to almost atmospheric level. However, since the microannulus is filled with water at a much higher pressure, and there is pressure support in the aquifer, the gas pressure at the aquifer is likely to be raised as well. This would stop the upward flow of the gas because the flow potential would increase at the aquifer level (h_2).

Assuming the top of the reservoir at 3000 m, and an aquifer at a depth of 1900 m (a conservative estimate for the area under study), we can estimate the gas flow potential for the conceptual model in Fig. 15. Table 4 summarizes the gas potential calculations. Initially, the water flow potential is zero at 3000 and 1900 m. As the reservoir depletes and water pressure declines, the water flow potential becomes negative. This indicates flow will occur from permeable aquifers into the reservoir through the microannulus. For gas however, the flow potential is positive at both depths. Initially, there is a strong flow potential difference between the reservoir and the aquifer, indicating a higher leakage rate. As the reservoir pressure declines from 30.8 to 28.5 MPa, the ΔΦ is still positive indicating gas leakage continues. As the reservoir depletes further, in this case to 19.1 MPa, the ΔΦ becomes negative and the leak stops. Therefore, there is a certain level of pressure depletion that can stop leakage due to buoyancy. This assessment depends strongly on the depth of the aquifer immediately above the caprock. If no such aquifer exists, then gas will continue leaking. Since the downward water rate is exceedingly small (according to our simulations 0.05 m^3/day), most formations with a permeability above 1 mD and 50 m thickness should be able to supply that water with little pressure drop over 100 years.

Table 4
Gas flow potential calculation for the conceptual model.

	ρ_g	$\Phi_{w@3000}$	$\Phi_{w@1900}$	$\Phi_{g@3000}$	$\Phi_{g@1900}$	ΔΦ
MPa	kg/m3	MPa	MPa	MPa	MPa	MPa
30.8	196	0.0	0	25.03	16.61	8.43
28.5	184	−1.5	0	23.09	16.61	6.48
19.1	128	−10.9	0	15.32	16.61	−1.29
12.0	80	−18.0	0	9.68	16.61	−6.92
7.3	47	−22.7	0	5.94	16.61	−10.67

Our simulations show that water flows into the reservoir through the microannulus at a rate of 20 m^3 per year (though the velocity is high as the microannulus is a small opening). This rate is too small to cause meaningful pressurization of gas around the well and lead to flow upwards along the microannulus. It is conceivable that as the water invades and pushes the gas away from the wellbore, it will isolate some gas bubbles in the pores and pressurize them. Therefore, in the near vicinity of the well, some bubbles may be able to get pressurized enough to flow upwards. However, this effect is very local and likely negligible as trapped gas bubbles also have an exceptionally low relative permeability in the near the well region.

The claim that depleted reservoirs are likely not a source of leakage is also supported by field measurements. Over 98% of the leaking wells in a large database from Alberta, Canada are likely sourced from shallow formations above the target reservoir (Bachu, 2017). This is likely due to the fact that target reservoirs are depleted, particularly close to the wells, and therefore leaks are less likely to stem from the target formations. The normally pressured formations above the target are the likely culprits for well leaks.

5.3. Shallow gas sources

Shallow gas-bearing formations can become sources of leaks in abandoned wells. The magnitude of the leaks depends on several parameters. The gas saturation at the source must be above the critical gas saturation for bulk flow to occur. Below the critical gas saturation, gas leakage is dominated by diffusive flow and is estimated to be below 20 kg/yr (Figs. 6 and 11) for the extremely damaged cement sheath considered in this work. This range is likely to be considered negligible by most jurisdictions, as no dissolved plume or free gas will accumulate in freshwater aquifers. For comparison, a dairy cow on average releases 100 kg/yr of methane (AEA, 1999).

The permeability of the leakage pathway is also a critical factor. If a viable source of gas is present, a mildly damaged cement sheath (1 md average permeability) will lead to relatively small leak rates. A high permeability leakage pathway must exist for concerning levels of leakage. An average damaged cement permeability of 100 md in this study shows leak rates of 3400 and 800 kg/yr into the Peelo aquifer and atmosphere, respectively (Figs. 8, 9, 12, and 13). MON-02 well is a notable example of a leaking well in the Netherlands (not the Groningen Field). For comparison, the estimated leak rate of the MON-02 was 3880 kg/yr into the atmosphere (Schout et al., 2019).

5.4. Methane plume

Leakage into freshwater aquifers can lead to the development of a methane plume near the well. This can impact the regional water quality and pose a risk of explosion if free gas accumulates. The results of the case study indicate that the dissolved methane plume can reach as far as 450 m horizontally away from the well after 100 years (Fig. 10), in the most extreme case considered. The free gas front will be behind the dissolved methane front, reaching as far as 350 m away from the well, after 100 years. These estimates do not consider the impact of groundwater flow velocity on the shape of the plume. Natural water seepage in freshwater aquifers can change the shape of the plume, extending it in the direction of flow and curtailing the plume in the opposite direction (Rice et al., 2018; Schout et al., 2020). Therefore, when designing monitoring locations for freshwater aquifers, the sampling location should be as close as possible to the well in the direction of groundwater flow, to ensure capturing the potential methane content in the samples. The sampling should be done in the most permeable confined aquifer, as the gas leaks into unconfined aquifers eventually escape to the atmosphere.

5.5. Intermediate formations

Methane molecules escaping the source formation flow upwards along the damaged cement sheath. The gas invades some formations along the way, depending on the pressure state, capillary entry pressure, and permeability of the formations. Therefore, the permeable intermediate formations could act as a storage for the leaked gas. This effect can be benign, if limited to a small area in an unproductive formation. However, if the intermediate formation is used for other operations, such as geothermal or storage activities, the hazards posed by the presence of a methane plume should be assessed.

Fig. 16 presents the rate of outflow of methane from the ORC formation for case 11 (extremely damaged cement). The total methane leakage into the atmosphere and Peelo aquifer is also presented on the plot. The results show that approximately 9000 kg/yr of methane flows out of the ORC. However, only 4000 to 4500 kg/yr enters the atmosphere-aquifer system. The rest of the leaked gas is stored in the intermediate formations between the ORC and the Peelo Formation. Ommelanden – top, Brussels Sand Member, and Breda Formation all store a portion of the leaked gas.

We have summarized the inflow/outflow rates of methane for the gas source, atmosphere/aquifers, and intermediate formations for several cases as presented in Table 5. The aim is to investigate the order of magnitude of the gas storage in the intermediate formation in various simulation cases. All the cases in Table 5 include an extremely damaged cement sheath (100 mD). Case 4 considers the reservoir at virgin pressure to be the source of gas. 850 kg/yr of methane escapes the reservoir, of which 800 kg/yr enters the atmosphere and the remaining gas enters the Peelo aquifer. Case 6 considers the same virgin-pressure reservoir and assumes the caprock is a no-flow boundary (no pressure interference from the caprock on the cement sheath). In case 6, the reservoir leaks 5200 kg/yr of methane;800 kg/yr leaks to the atmosphere while 3400 kg/yr enters the Peelo aquifer. The remaining 1000 kg/yr of gas is stored in intermediate formations. Case 11 assumes the ORC to be the source of gas, where 8900 kg/yr of methane leaks. The leak rate into the atmosphere and Peelo are 800 and 3400 kg/yr, respectively, similar to case 6. However, a larger portion of the leaked gas is stored in the intermediate formations. Cases 14 and 16 show that having an over-pressured gas source can significantly increase the leakage rate out of the source, however in the present system it is entirely taken up by the intermediate formations. This explains the results in Fig. 13, where an increase in source pressure does not increase the leak rate into the atmosphere or the Peelo aquifer. These results show that the intermediate formations can play a vital role in capping the leakage rates into the atmosphere and freshwater aquifers. The role of intermediate aquifers has also been discussed in the context of CO2 leakage (Cihan et al., 2013). In the present system, the atmosphere is the first recipient of the leaked gas. Once the leak rate reaches approximately 800 kg/yr, the pressure in the cement sheath overcomes the capillary entry pressure of the Peelo aquifer. The extra leakage rate is then stored in the Peelo aquifer, until the rate of 3400 kg/yr is reached. Past this point, the additional leakage is stored in the intermediate formations. The relative impact of the intermediate formations depends on their capillary entry pressure and permeability, relative to the freshwater aquifers. A lack of permeable intermediate formations could exacerbate the leakage rates into aquifers and atmosphere if a gas source and a leakage pathway already exist.

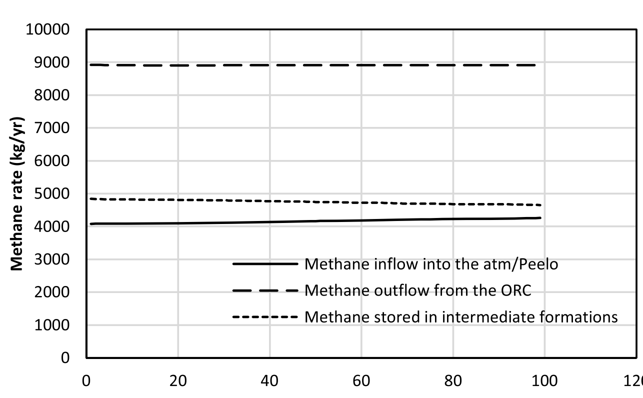

Fig. 16. The rate of methane outflow from the ORC, compared to the stored methane in the intermediate formations (case 11).

In this study, the permeability of the cement sheath was assumed to be uniform along the pathway. This may not be reflective of the field conditions. The cement sheath can be comprised of multiple undamaged and damaged zones that in combination exhibit an average permeability across the length of the well. Depending on the location of the undamaged zones, the distribution of the leaked volume could vary. For example, the presence of a long undamaged section of cement below the aquifer may direct a higher proportion of the leaked gas into the deeper intermediate formation, compared to the atmosphere or the aquifers. The impact of non-uniform cement damage is not in the scope of this study. This impact can be studied using the present methodology by incorporating Cement Bond Logs (CBL) or Ultrasonic logs to estimate the distribution of damage along the cement sheath. This can better identify the locations of high risk gas accumulations in the subsurface for a particular well.

5.6. Leakage risk

The findings of this work provide a blueprint to assess gas leakage risk through abandoned wells. The results can be used to identify high-risk wells and to determine appropriate monitoring, or remediation strategies. The abandoned gas fields below a certain pressure threshold will not be a likely source of gas leaks unless there is evidence of re-pressurization. Therefore, potential shallow gas sources should attract the most attention. Unfortunately, these non-productive gas-bearing formations are usually not well-characterized. Estimates of gas saturation, permeability, and capillary pressure are needed to assess whether these formations could become a source of leakage. Once a potential source is identified, the effort should be focused on the wells that can have elevated levels of cement damage. Wells that have experienced significant pressure and temperature shocks, exposed to corrosive compounds, used poor cementing recipes or technologies can be high-risk candidates (Bachu, 2017; King and King, 2013). Presence of a normally or over-pressured gas source and a leakage pathway signals a high likelihood of leakage. The presence of permeable intermediate formations can provide a buffer zone and cap the leak rate into the atmosphere or freshwater aquifers. Monitoring campaigns may be needed to estimate the leakage rates in the atmosphere or aquifers for high-risk wells, to assess whether remediation is required.

6. Conclusions

In this work, a numerical study was conducted on gas leakage from abandoned wells in the Groningen Field. The model included the main reservoir, intermediate formations, freshwater aquifers, the atmosphere (as a boundary condition), and the leakage pathway. The impact of reservoir pressure and the presence of shallow gas sources were investigated. The following conclusions can be drawn from this study:

- A depleted reservoir is not a likely source of gas leakage, as long as its pressure remains below a certain threshold that depends on the local subsurface conditions. This indicates that buoyancy and diffusive flow are not sufficient to cause significant leak rates in depleted reservoirs. Shallow gas-bearing formations are more likely to act as a leakage source if the permeability is sufficiently high and the gas saturation is above-critical to lead to bulk flow.

Table 5
Summary of methane inflow and outflow for the gas sources, the atmosphere/aquifers, and the intermediate formations. All cases presented have extremely damaged cement sheath (see Table 3 for the description of the cases). The reported values below are average leakage rates over 100 years.

Case no.	Gas source	Condition	Source outflow	Atm/aquifers inflow	Intermediate formations inflow	Leakage to atmosphere	leakage to Peelo
			kg/yr	kg/yr	kg/yr	kg/yr	kg/yr
4	Reservoir	Reservoir at virgin pressure (34.5 MPa)	850	850	0	800	50
6	Reservoir	Reservoir at virgin pressure (34.5MPa), caprock blocks disabled (no pressure barrier)	5200	4200	1000	800	3400
11	ORC	Base case for Organic-rich claystone as source	8900	4200	4700	800	3400
13	ORC	Higher permeability (50 md) for ORC	8900	4200	4700	800	3400
14	ORC	ORC assumed to be over-pressured by 10%	110,000	4200	105,800	800	3400
16	ORC	ORC assumed to be over-pressured by 10%, with a high permeability (50 md)	110,000	4200	105,800	800	3400

- For a mildly damaged cement sheath with an average permeability of 1 md, all scenarios show relatively low levels of gas leakage. The leakage rate for the present case study is estimated to be less than 20 kg/yr, well below average emissions of a dairy cow (100 kg/year). The plume size in the freshwater aquifer is also expected to be negligible.
- A high permeability leakage pathway (100 mD) can lead to significant leakage rates if a productive gas source is present. The simulation results show that for the system under study, the dissolved methane plume can travel as far as 450 m away from the wellbore in the Peelo aquifer, after 100 years. The expected leakage rates into the Peelo aquifer and atmosphere are expected to be 3400 kg/yr, and 800 kg/yr, respectively, for the most extreme case considered. Unconfined aquifers such as the Boxtel Formation do not store significant amounts of gas, as the invading gas ultimately escapes to the atmosphere.
- Permeable intermediate formations between the source and aquifers can act as a gas storage buffer. These formations can be critical in limiting the maximum rate of leakage into the atmosphere and freshwater aquifers. Capillary entry pressure and the permeability of the intermediate formations relative to the freshwater aquifers can determine the effectiveness of the leak buffer.

CRediT authorship contribution statement

Al Moghadam: Conceptualization, Methodology, Writing – original draft, Visualization, Validation. **Elisabeth Peters:** Conceptualization, Investigation, Validation, Resources, Writing – review & editing. **Susanne Nelskamp:** Investigation, Resources.

Declaration of Competing Interest

This work was funded by the Dutch Ministry of Economic Affairs and Climate Policy. The authors declare that they have no known competing financial interests or personal relationships that could have appeared to influence the work reported in this paper.

Data availability

Data will be made available on request.

Acknowledgements

The work presented here has been carried out as part of the KEM-19 project. The KEM (Knowledge Programme on Effects of Mining) projects are a part of the Dutch national research program, initiated by the Ministry of Economic Affairs and Climate Policy. We would like to thank Majid Hassanizadeh, Karin van Thienen-Visser, Ane Wiersma, and Kevin Parks for constructive discussions and revisions.

References

Abboud, J.M., Watson, T.L., Ryan, M.C., 2021. Fugitive methane gas migration around Alberta's petroleum wells. Greenhouse Gas Sci. Technol. 11, 37–51.
AEA, 1999. Options to reduce methane emissions. Final report: aEAT-3773 prepared for DGXI.
Bachu, S., 2017. Analysis of gas leakage occurrence along wells in Alberta, Canada, from a GHG perspective – Gas migration outside well casing. Int. J. Greenh. Gas Control 61, 146–154.
Bachu, S., Watson, T.L., 2006. Possible indicators of leakage along wells. In: Proceeding of the 8th Conference on Greenhouse Gas Control Technologies (GHGT-8). Trondheim, Norway. June 19–22, 2006.
Bachu, S., Bennion, D.B., 2009. Experimental assessment of brine and/or CO2 leakage through well cements at reservoir conditions. Int. J. Greenhouse Gas Control 3, 494–501.
Békési, E., Struijk, M., Bonté, D., Veldkamp, H., Limberger, J., Fokker, P.A., Vrijlandt, M., van Wees, J.D., 2020. An updated geothermal model of the Dutch subsurface based on inversion of temperature data. Geothermics 88, 101880.
Bois, A.-P., Garnier, A., Rodot, F., Sain-Marc, J., Aimard, N., 2011. How to prevent loss of zonal isolation through a comprehensive analysis of microannulus formation. SPE Drill. Completion 26 (01), 13–31.
Bonté, D., van Wees, J.-D., Verweij, H., 2012. Subsurface temperature of the onshore Netherlands: new temperature dataset and modellin. Netherlands J. Geosci. 91 (4), 491–515.
Böttner, C., Haeckel, M., Schmidt, M., Berndt, C., Vielstädte, L., Kutsch, J.A., Karstens, J., Weiß, T., 2020. Greenhouse gas emissions from marine decommissioned hydrocarbon wells: leakage detection, monitoring and mitigation strategies. Int. J. Greenh. Gas Control 100, 103119.
Brooks, R.H., Corey, A.T., 1964. Hydraulic properties of porous media. In: Hydrology Papers, 3. Colo. State Univ., Fort Collins, p. 37.
Burkitov, U., H. van Oeveren and P. Valvatne, 2016. Groningen Field Review 2015. Subsurface Dynamic Modelling Report. https://www.nam.nl/feiten-en-cijfers.html.
Carroll, S.A., Keating, E., Mansoor, K., Dai, Z., Sun, Y., Trainor-Guitton, W., Brown, C., Bacon, D., 2014. Key factors for determining groundwater impacts due to leakage from geologic carbon sequestration reservoirs. Int. J. Greenhouse Gas Control 29, 153–168.
Cihan, A., Birkholzer, J.T., Zhou, Q., 2013. Pressure buildup and brine migration during CO2 storage in multilayered aquifers. Groundwater 51, 252–267.
Collins, D.A., Grabenstetter, J.E., Sammon, P.H., 2003. A shared-memory parallel black-oil simulator with a parallel ILU linear solver. In: SPE 79713, SPE Reservoir Simulation Symposium. Houston, TX. February 3-5.
Conference Board of Canada, 2011. Greenhouse Gas (GHG) Emissions. http://www.conferenceboard.ca/hcp/details/environment/greenhouse-gas-emissions.aspx.
Crow, W., Carey, J.W., Gasda, S., Williams, D.B., Celia, M.A., 2010. Wellbore integrity analysis of a natural CO2 producer. Int. J. Greenhouse Gas Control 4 (2), 186–197.
Darrah, T.H., Vengosh, A., Jackson, R.B., Warner, N.R., Poreda, R.J., 2014. Noble gases identify the mechanisms of fugitive gas contamination in drinking-water wells overlying the Marcellus and Barnett Shales. Proc. Natl. Acad. Sci. 111, 14076–14081.
Davies, R.J., Almond, S., Ward, R.S., Jackson, R.B., Adams, C., Worrall, F., et al., 2014. Oil and gas wells and their integrity: implications for shale and unconventional resource exploitation. Mar. Pet. Geol. 56, 239–254.
From: Doornenbal, J.C., Kombrink, H., Bouroullec, R., Dalman, R.A.F., de Bruin, G., Geel, C.R., Houben, A.J.P., Jaarsma, B., Juez-Larré, J., Kortekaas, M., Mijnlieff, H.F., Nelskamp, S., Pharaoh, T.C., ten Veen, J.H., ter Borgh, M., van Ojik, K., Verreussel, R.M.C.H., Verweij, J.M., Vis, G.-J., 2019. New insights on subsurface energy resources in the Southern North Sea Basin area. In: Patruno, S., Archer, S.G., Chiarella, D., Howell, J.A., Jackson, C.A.-L., Kombrink, H. (Eds.), Cross-Border Themes in Petroleum Geology I: The North Sea. Geological Society, London, Special Publications, p. 494. https://doi.org/10.1144/SP494-2018-178.
El Hachem, K., Kang, M., 2022. Methane and hydrogen sulfide emissions from abandoned, active, and marginally producing oil and gas wells in Ontario, Canada. Sci. Total Environ. 823, 153491.
Gasda, S.E., Celia, M.A., Wang, J.Z., Duguid, A., 2013. Wellbore permeability estimates from vertical interference testing of existing wells. Energy Procedia 37, 5673–5680.

Gasda, S.E., Bachu, S., Celia, M.A., 2004. Spatial characterization of the location of potentially leaky wells penetrating a deep saline aquifer in a mature sedimentary basin. Environ. Geol. 46, 707–720.
Grötsch, J., Sluijk, A., van Ojik, K., de Keijzer, M., Graaf, J., Steenbrink, J., 2011. The Groningen gas field: fifty years of exploration and gas production from a Permian dryland reservoir. SEPM Spec. Publ. 98, 11–33.
Harrison, S.S., 1983. Evaluating system for ground-water contamination hazards due to gas-well drilling on the glaciated Appalachian plateau. Groundwater 21, 689–700.
Hagoort, J., 1988. Fundamentals of gas reservoir engineering. In: Developments in Petroleum Science, 23. Elsevier, Amsterdam.
Harvey, A.H., 1996. Semiempirical correlation for Henry's constants over large temperature ranges. AIChE J. 42, 1491–1494.
Harvey, O.R., Qafoku, N.P., Cantrell, K.J., Lee, G., Amonette, J.E., Brown, C.F., 2013. Geochemical implications of gas leakage associated with geologic CO2 storage - a qualitative review. Environ. Sci. Technol. 47, 23–36.
Huet, C.C., Rushing, J.A., Newsham, K.E., Blasingame, T.A., 2005. A modified Purcell/Burdine model for estimating absolute permeability from mercury injection capillary pressure data. In: paper IPTC 10994 presented at the 2005 International Petroleum Technology Conference. Doha. The Am. Assoc. of Pet. Geol., 21–23 Nov.
Ingraffea, A.R., Wells, M.T., Santoro, R.L., Shonkoff, S.B.C., 2014. Assessment and risk analysis of casing and cement impairment in oil and gas wells in Pennsylvania, 2000–2012. Proc. Natl. Acad. Sci. 111, 10955–10960. https://doi.org/10.1073/pnas.1323422111.
From Jager, J.de, Geluk, M.C., 2007. Petroleum geology. In: Wong, T.E., Batjes, D.A.J., Jager, J.D. (Eds.), Geology of the Netherlands, pp. 241–264.
Jager, J.D., Visser, C., 2017. Geology of the Groningen field – an overview. Netherland J. Geosci. 96 (5), 3–15.
J.R. Fanchi, in Principles of applied reservoir simulation (4th Edition), 2018.
Jossi, J.A., Stiel, L.I., Thodos, G., 1962. The viscosity of pure substances in the dense gaseous and liquid phases. AIChE J. 8, 59–63.
Kang, M., Baik, E., Miller, A.R., Bandilla, K.W., Celia, M.A., 2015. Effective permeabilities of abandoned oil and gas wells: analysis of data from Pennsylvania. Environ. Sci. Technol. 49 (7), 4757–4764.
Kang, M., Christian, S., Celia, M.A., Mauzerall, D.L., Bill, M., Miller, A.R., et al., 2016. Identification and characterization of high methane-emitting abandoned oil and gas wells. Proc. Natl. Acad. Sci. 113 (48), 13636–13641.
Kang, M., Kanno, C.M., Reid, M.C., Zhang, X., Mauzerall, D.L., Celia, M.A., et al., 2014. Direct measurements of methane emissions from abandoned oil and gas wells in Pennsylvania. Proc. Natl. Acad. Sci. 111 (51), 18173–18177.
Keating, E., Newell, D., Dempsey, D., Pawar, R., 2014. Insights into inter-connections between the shallow and deep systems from a natural CO2 reservoir near Springerville, Arizona. Int. J. Greenh. Gas Control 25, 162–172.
Kelly, W.R., Matisoff, G., Fisher, J.B., 1985. The effects of a gas well blow out on groundwater chemistry. Environ. Geol. Water Sci. 7, 205–213.
Kestin, J., Khalifa, H.E., Correia, R.J., 1981. Tables of the dynamic and kinematic viscosity of aqueous NaCl solutions in the temperature range 20-150°C and pressure range 0.1-35 MPa. J. Phys. Chem. Ref. Data 10, 71–87.
King, G.E., King, D.E., 2013. Environmental risk arising from well-construction failure-differences between barrier and well failure, and estimates of failure frequency across common well types, locations, and well age. SPE Prod. Oper. 28 (4), 323–344.
Li, K., Horne, R.N., 2006. Comparison of methods to calculate relative permeability from capillary pressure in consolidated water-wet porous media. Water Resour. Res. 42, W06405.
Lopez, O., Berg, C.F., Bakke, S., Boassen, T., Rustad, A.B., 2013. Thin section image analysis for estimation of initial water saturation in siliciclastic reservoir rocks. In: Paper presented at the International Symposium of the Society of Core Analysts held in Napa Valley, California, USA, 16-19 September.
McMahon, P.B., Thomas, J.C., Crawford, J.T., Dornblaser, M.M., Hunt, A.G., 2018. Methane in groundwater from a leaking gas well, Piceance Basin, Colorado, USA. Sci. Total Environ. 634, 791–801.
Meng, M., Frash, L.P., Carey, J.W., Li, W., Welch, N.J., Zhang, W., 2021. Cement stress and microstructure evolution during curing in semi-rigid high-pressure environments. Cem. Concr. Res. 149, 106555.
Ministry of Economic Affairs and Climate Policy, Natural resources and geothermal energy in the Netherlands - Annual review 2019. https://www.nlog.nl/sites/default/files/2020-11/annual_review_2019_natural_resources_and_geothermal_energy_en_18-11-2020.pdf.
Moghadam, A., Castelein, K., ter Heege, J., Orlic, B., 2022. A study on the hydraulic aperture of microannuli at the casing-cement interface using a large-scale laboratory setup. Geomechan. Energy Environ. 29, 100269.
Moghadam, A., Castelein, K., ter Heege, J., van der Valk, K., Orlic, B., Wollenweber, J., 2020. Large-scale laboratory investigation of the microannulus behavior in the casing-cement interface. In. In: Proceedings of the 54th US Rock Mechanics /Geomechanics Symposium (ARMA), ARMA 20-1325.
Nghiem, L.X., Li, Y.-K., 1989. Phase-Equilibrium Calculations for Reservoir Engineering and Compositional Simulation. In: Second International Forum on Reservoir Simulation. Alpbach, Austria. September 4-8.
Nowamooz, A., Lemieux, J.M., Molson, J., Therrien, R., 2015. Numerical investigation of methane and formation fluid leakage along the casing of a decommissioned shale gas well. Water Resour. Res. 51 (6), 4592–4622.
Omara, M., Sullivan, M.R., Li, X., Subramanian, R., Robinson, A.L., Presto, A.A., 2016. Methane emissions from conventional and unconventional natural gas production sites in the Marcellus Shale Basin. Environ. Sci. Technol. 50 (4), 2099–2107.
Orlic, B., Chitu, A., Brunner, L., Koenen, M., Wollenweber, J., Schreppers, G.-J., 2018. Numerical investigations of cement interface debonding for assessing well integrity risks. In: Proceedings of the 52nd US Rock Mechanics /Geomechanics Symposium (ARMA), Seattle, Washington, 17-20 June 2018. ARMA 18-1298.
Osborn, S.G., Vengosh, A., Warner, N.R., Jackson, R.B., 2011. Methane contamination of drinking water accompanying gas-well drilling and hydraulic fracturing. Proc. Natl. Acad. Sci. U. S. A. 108 (20), 8172–8176.
Pekney, N.J., Diehl, J.R., Ruehl, D., Sams, J., Veloski, G., Patel, A., Schmidt, C., Card, T., 2018. Measurement of methane emissions from abandoned oil and gas wells in Hillman State Park, Pennsylvania. Carbon Manage. 9 (2), 165–175.
Peng, D.Y., Robinson, D.B., 1976. A new two-constant equation of state. Ind. Eng. Chem. Fundamen. 15, 59–64.
Postma, T.J.W., Bandilla, K.W., Celia, M.A., 2019. Estimates of CO2 leakage along abandoned wells constrained by new data. Int. J. Greenhouse Gas Control 84, 164–179.
Reagan, M.T., Moridis, G.J., Keen, N.D., Johnson, J.N., 2015. Numerical simulation of the environmental impact of hydraulic fracturing of tight/shale gas reservoirs on near surface groundwater: background, base cases, shallow reservoirs, short-term gas, and water transport. Water Resour. Res. 51 (4), 2543–2573.
Rice, A.K., McCray, J.E., Singha, K., 2018. Methane leakage from hydrocarbon wellbores into overlying groundwater: numerical investigation of the multiphase flow processes governing migration. Water Resour. Res. 54, 2959–2975.
Rowe, A.M., Chou, J.C.S., 1970. Pressure-volume-temperature-concentration relation of aqueous NaCl solutions. J. Chem. Eng. Data 15, 61–66.
Roy, P., Morris, J.P., Walsh, S.D.C., Iyer, J., Carroll, S., 2018. Effect of thermal stress on wellbore integrity during CO2 injection. Int. J. Greenh. Gas Con. 77, 14–26.
Schout, G., Griffioen, J., Hassanizadeh, S.M., Cardon de Lichtbuer, G., Hartog, N., 2019. Occurrence and fate of methane leakage from cut and buried abandoned gas wells in the Netherlands. Sci. Total Environ. 659, 773–782.
Schout, G., Hartog, N., Hassanizadeh, M., Helmig, R., Griffioen, J., 2020. Impact of groundwater flow on methane gas migration and retention in unconsolidated aquifers. J. Contam. Hydrol. 230, 103619.
SGS Horizon BV, 2016. Independent Review of Groningen Subsurface Modelling, Update for Winningsplan 2016 with Opinion Letter. https://www.nam.nl/over-nam/onderzoeksrapporten.html.
Shi, S., Belhaj, H., Bera, A., 2018. Capillary pressure and relative permeability correlations for transition zones of carbonate reservoirs. J. Petrol Explor. Prod. Technol. 8, 767–784.
Stormont, J.C., Fernandez, S.G., Taha, M.R., Matteo, E.N., 2018. Gas flow through casing-cement microannuli under varying stress conditions. Geomech. Energy Env. 1, 1–13.
Tao, Q., Bryant, S.L., 2014. Well permeability estimation and CO2 leakage rates. Int. J. Greenhouse Gas Control 22, 77–87.
Thomas, G.W., Thurnau, D.H., 1983. Reservoir Simulation Using an Adaptive-Implicit Method. SPEJ 23, 759–768. October.
TNO and Deltares, 2022. KEM-19 Evaluation of post-abandonment fluid migration and ground motion risks in subsurface exploitation operations in the Netherlands. Phase 2, 158 p.
TNO, 2015. Report R10056. TNO, p. 83.
TNO-GDN, 2022. Breda Formation. Stratigraphic Nomenclature of the Netherlands. TNO – Geological Survey of the Netherlands. Accessed on 03-02-2022 from. http://www.dinoloket.nl/en/stratigraphic-nomenclature/breda-formation.
US EPA, 2017. Greenhouse gas emissions reporting from the petroleum and natural gas industry - background technical support document.
van Elk, J., Landmann, A.J., van Eijs, R., 2021. Reservoir Pressure and Subsidence Groningen Field update for Production Profile GTS – raming 2021. https://www.nam.nl/over-nam/onderzoeksrapporten.html.
Verweij, H., Simmelink, E., Underschultz, J. (2011) Pressure and fluid flow systems in the Permian Rotliegend in the Netherlands onshore and offshore. From The Permian Rotliegend of the Netherlands. SEPM Special Publication No. 98. pp. 247–263.
Vielstädte, L., Haeckel, M., Karstens, J., Linke, P., Schmidt, M., Steinle, L., Wallmann, K., 2017. Shallow gas migration along hydrocarbon wells–an unconsidered, anthropogenic source of biogenic methane in the North Sea. Environ. Sci. Technol. 51 (17), 10262–10268.
Vielstädte, L., Karstens, J., Haeckel, M., Schmidt, M., Linke, P., Reimann, S., et al., 2015. Quantification of methane emissions at abandoned gas wells in the Central North Sea. Mar. Pet. Geol. 68, 848–860.
Wang, L., Cardenas, M.B., 2018. Connecting pressure-saturation and relative permeability models to fracture properties: the case of capillary-dominated flow of supercritical CO2 and brine. Water Resour Res. 54, 6965–6982. https://doi.org/10.1029/2018WR023526.
Wang, Y., Wu, C., Zhou, Y., 2017. Effect study of aperture distribution on the capillary pressure-saturation relation for the single fracture. Geofluids 2017, 9656393. https://doi.org/10.1155/2017/9656393.
Watson, T.L., Bachu, S., 2009. Evaluation of the potential for gas and CO2 leakage along wellbores. SPE Drill. Completion 24 (1), 115–126.
Watson, T.L., Bachu, S., 2008. Identification of wells with high CO2-leakage potential in mature oil fields developed for CO2-enhanced oil recovery. In: Paper SPE 112924 presented at the SPE Symposium on Improved Oil Recovery. Tulsa, Oklahoma, USA, 20-23 April.
Wilke, C.R., Chang, P., 1955. Correlation of diffusion coefficients in dilute solution. AIChE J. 1, 264–270. June.
Williams, J.P., Regehr, A., Kang, M., 2021. Methane emissions from abandoned oil and gas wells in Canada and the United States. Environ. Sci. Technol. 55 (1), 563–570. https://doi.org/10.1021/acs.est.0c04265.